

## Chapter 23

# Miniaturized Reactor Concepts and Advanced Analytics for Primary Screening in High-Throughput Experimentation

Torsten Zech, Jens Klein, Stephan A. Schunk, Thorsten Johann,  
Ferdinand Schüth, Stefan Kleditzsch, and Olaf Deutschmann

### INTRODUCTION

The development of novel and better catalysts for chemical processes is mainly an empirical process utilizing existing technical expertise and experience. The aim of reducing time and costs has proved a powerful incentive for the development of high-throughput technologies for applications in heterogeneous and homogeneous catalysis.

Obviously, there are strong analogies between the development of combinatorial chemistry for drug discovery and combinatorial materials science, of which *high throughput experimentation* in catalysis is an important part. It is worth reading the excellent paper by Lebl [1] about the development of combinatorial chemistry and comparing it with today's situation in combinatorial material science and high-throughput experimentation. The first papers in combinatorial chemistry were published in the mid-eighties. Since then, activities in this field have grown exponentially, fundamentally changing old research paradigms. The first companies operating in this field were founded during the late eighties

**Torsten Zech, Jens Klein, and Stephan A. Schunk** • hte Aktiengesellschaft, Kurpfalzring 104, 69123 Heidelberg, Germany

**Thorsten Johann and Ferdi Schüth** • Max-Planck-Institut für Kohlenforschung, Kaiser-Wilhelm-Platz 1, 45470 Mülheim an der Ruhr, Germany

**Stefan Kleditzsch** • Universität Heidelberg, Interdisziplinäres Zentrum für Wissenschaftliches Rechnen, Im Neuenheimer Feld 368, 69120 Heidelberg, Germany

**Olaf Deutschmann** • Institut für Chemische Technik, Universität Karlsruhe, Kaiserstr. 12, D-76131 Karlsruhe, Germany

and at the beginning of the nineties. Nowadays, combinatorial chemistry and high-throughput screening are core technologies in all major pharmaceutical companies.

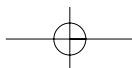
In addition, parallel testing technologies have been used for a long time in materials science [2] and *heterogeneous catalysis* [3, 4]. Nevertheless, on the landmark publication by Xiang et al. in 1995 [5] attracted a great deal of attention. Since then, numerous applications of library screening techniques for the different stages in the development of heterogeneous catalysts have been reported [6–15]. Approaches to high-throughput experimentation in catalysis are generally divided into two stages: *catalyst discovery (primary screening)* as the first stage, and *catalyst optimization (secondary screening)* as the second stage.

The main target in primary screening is the identification of hits out of large catalyst libraries. The number of catalysts tested in parallel should be a few hundred on a small reactor footprint. Therefore, specific library preparation methods resulting in very small amounts of the individual materials are required. The depth of information of the analytical methods employed is often reduced in favor of a high analytical speed. Accordingly, only the most promising materials from a library are characterized in order to gain additional insights into their properties. Primary screening approaches are usually employed in ambitious catalyst discovery programs with little or no previous knowledge about the target reaction and the class of materials to be studied.

In contrast, the secondary screening of catalytic materials aims at optimization of known catalyst formulations and reaction conditions at a more sophisticated level. Results and relations discovered in primary screening are explored in more detail in all phases of the work flow, encompassing (1) increasing the quantities of catalysts prepared by conventional synthesis procedures, (2) more detailed screening processes involving wide variation and precise control of reaction parameters, (3) complete and accurate product analysis, and (4) careful characterization of the tested materials. In all phases of a secondary screening work flow, the conditions are “close to conventional” compared with standard “one catalyst at a time” testing procedures.

Catalyst preparation is carried out predominantly by well-known conventional methods (e.g., impregnation, precipitation, ion exchange). In most cases, a large number of parallel fixed-bed reactors, each filled with 20–200 mg of catalyst, is operated in parallel under a specific set of steady state operating conditions and continuous flow. Product analysis is generally carried out in a sequential manner by well-established analytical methods (e.g., gas chromatography, gas chromatography–mass spectrometry, or Fourier transform IR spectroscopy) using multiposition valves for channel selection. If carefully designed and operated, the performance of secondary screening reactors is similar to or better than that of conventional laboratory reactors.

Because of the successful application of secondary screening tools, the demand for primary screening devices and methodologies has increased, with miniaturization being one of the key issues. However, only a few primary screening techniques are described in the literature, with a strong focus on the applied analysis technique. In the first publication in the field, Moates et al. [6] used a simple setup comprising a substrate-based library and an IR camera to detect catalytic activity. Holzwarth et al. [8] extended this principle to emission-corrected IR thermography with high-temperature resolution to resolve reaction heats spatially over catalyst libraries composed of transition metals in amorphous microporous mixed oxides on a flat substrate over which the reactants



flowed. Obviously, this technique cannot be used to identify reaction products and thus estimate selectivities, but it is particularly useful for detecting catalyst activity sensitively and effectively during primary screening. Flat substrates with catalysts produced as thin films were also used by Cong et al. [9]. Two concentric capillaries were used to supply and withdraw reactants, and the catalysts were tested sequentially in a transient mode with a special mass spectrometer. Later, this methodology was simplified and extended by Orschel et al. [12], who used small amounts of catalyst particles deposited in wells on the substrate. The reactor characteristics were also improved, allowing a conventional mass spectrometer to be used. However, the catalysts were still tested in a sequential and transient mode. Thus it was not possible to follow activation and deactivation phenomena over long periods of time. Senkan [7] developed the resonance-enhanced multiphoton ionization method (REMPI) to detect a selected molecule in the effluent of a continuously operated arrangement of fixed-bed catalysts and a multi-chamber reactor system [16]. The products are detected by an array of spatially addressable microelectrodes directly exposed to the gas stream after the absorption and ionization features of the target molecule have been determined. However, this can cause problems in measurements over a long period because of drift of the electrode response. Furthermore, the system has not been miniaturized to allow larger catalyst libraries to be tested simultaneously. Another interesting technique used for primary screening is photothermal deflection [17], which allows fast sequential analysis based on two crossed laser beams.

Techniques based on optical readout of catalyst activity are very suitable for real-time parallel deflection since first analysis is possible. The first use of this approach was by Reddington et al. [18], who used fluorescence detection of protons formed at the anode catalyst of a direct methanol fuel cell by a fluorescent dye. This work was carried out in solution where the lack of mixing allowed the fluorescence signal to be correlated with the catalyst, but direct parallel analysis of products is also possible in a gas stream from a parallel reactor. A selective reaction of the product or an educt of the reaction with a selective color reagent is used to do this [19]. Such a system, which can be parallelized to a rather high degree, has recently been used to detect NO remaining in the offstream of potential DeNO<sub>x</sub> catalysts arranged in a 49-channel parallel reactor [20].

As can be seen, one of the crucial elements of a primary screening setup is an analysis technique which is able to deal with very low sample volumes while providing good spatial resolution and sufficient chemical information about the nature and amount of the products. Generally, fast sequential, quasiparallel and parallel analysis techniques can be distinguished. Usually, simple parallel detection methods such as IR thermography [6,8] provide a lower depth of information than sequential methods like mass spectrometry [21], but are lot faster.

Primary screening approaches also require an integration of catalyst preparation, reactor, and analysis methods. This may result in unconventional preparation methods or reaction conditions that complicate the transfer of results from primary to secondary screening. In addition, the question of miniaturization so that several hundred catalysts can be tested simultaneously has not yet been addressed sufficiently, although it is known from combinatorial and analytical chemistry that miniaturized reactors and microfluidics can be applied successfully. One reason for this is related to the challenging requirements that have to be met by primary screening reactors: the reactor design has to accommodate

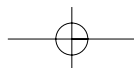
catalysts made by a simple, fast, and scalable catalyst preparation method; many catalysts should be tested simultaneously under steady state conditions and continuous flow; and the analysis method should have a high spatial resolution and allow a good estimate of conversion degree and selectivity, while still being very fast and reproducible.

Although microstructured reactors have attracted a great deal of interest in recent years, little is known about continuously operated miniaturized reactors for applications in high-throughput discovery programs in catalysis. Jensen and co-workers recently presented a novel differential packed-bed microreactor designed for the investigation of heterogeneously catalyzed gas phase reactions [22,23]. Utilization of the reactor for the determination of the reaction kinetics of CO oxidation on a Pd–Al<sub>2</sub>O<sub>3</sub> catalyst was discussed. The proposed cross-flow design led to a uniform flow distribution over the catalyst bed, which was confirmed by a two-dimensional computational fluid dynamics (CFD) simulation based on a finite-element approach. The authors state that this type of reactor could also be applied to high-throughput testing of heterogeneous catalysts, although no example is given.

Another approach was explored by Bergh et al. [24], who used an arrangement of reaction chambers with thin- or thick-film catalysts on a flat substrate for parallel catalyst testing. These workers also described a method for continuously supplying reactants to the reaction chambers [25]. However, the description of the actual design of the reactor is not unambiguous, which makes a technical evaluation of this approach difficult.

From our own experience with microchannel-based approaches for catalyst discovery [26,27] we concluded that microstructured reactors present a number of interesting properties which are worth investigating with respect to primary screening. Microstructured reactors provide excellent heat and mass transfer properties and can be operated at isothermal conditions. The response times to changes of the reaction conditions are very low and a number of additional static or active elements (mixers, valves, etc.) can be integrated into the device besides the reactor itself. Owing to their potential mass fabrication, miniaturized reactors may prove cost efficient. However, much development work is necessary to set up a microstructured reactor system, as many microfabrication technologies are still being considered “experimental” and the behavior of miniaturized reactors is still not well understood.

Therefore the application of CFD calculations should be considered to facilitate system design. A variety of commercial and academic computational tools which can assist in the development and design of reactors for heterogeneously catalyzed gas phase reactions have been developed in the last few years. CFD codes which can numerically predict the flow field, the temperature, and species concentration distributions in three-dimensional configurations, sometimes even including detailed models for the heterogeneous reactions on the catalytic surface and potential homogeneous reactions in the gas phase, are also available [28]. Provided that the assumptions of continuum mechanics remain valid, these tools can be used to simulate processes in microreactors. A frequent advantage of small reactors is that the flow field remains laminar; thus no turbulence model needs to be applied. For instance, CFD simulations have led to a better understanding of the reactive flows in the small channels (radius 125–500 μm) of catalytic monoliths [29,30] and around catalytic wires [31–33] for selective oxidation reactions and microburners [34–36].



## “SINGLE-BEAD REACTORS” FOR PRIMARY CATALYST SCREENING

### Catalytic Materials and Reactor Architecture

The basis of the *single-bead concept* is the use of single *shaped bodies* as the catalytic material of interest. In principle, these particles may be of any shape, but are usually spherical. In accordance with approaches known from combinatorial chemistry, such spherical particles are called “*beads*”, although they fulfil very different functions in comparison with their application in combinatorial setups in organic and biochemistry.

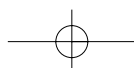
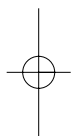
Each bead represents one catalyst as a member of a library of *solid catalysts*. It consist of an nonporous material (e.g.,  $\alpha$ -Al<sub>2</sub>O<sub>3</sub> or Steatit) or a typical porous support material (e.g.,  $\gamma$ -Al<sub>2</sub>O<sub>3</sub>, SiO<sub>2</sub>, or TiO<sub>2</sub>). These beads can be subjected to different synthesis procedures and sequences such as impregnation, coating, etc. In addition, full mixed metal oxide catalysts can also be formed to spherical particles.

Using single beads for *high-throughput experimentation* has a number of advantages. First, such beads are comparable to well-known fixed bed catalysts and the synthesis pathways can be the same as for conventional materials, which may facilitate scale-up procedures. A number of common preparation procedures, which can be carried out in standard laboratory environments, are available for these beads.

The second main advantage is that each bead represents a single entity that can be handled independently from other beads or the final reactor configuration. Starting from master batches, a large diversity of materials can easily be prepared. Furthermore, different beads can be treated individually, for instance, subjected to different preparation steps or pretreatments like calcination or steaming, rather than handling the complete library as is necessary for substrate-bound thin- or thick-film catalysts. This property allows the use of synthesis procedures different from the parallel approach. Furthermore, the potential use of *ex situ synthesis* procedures may present a significant advantage, especially in *microchemical systems*, as in situ preparation of the catalysts in the reactor could cause problems with contamination or the thermal and chemical stability of the reactor material.

The reactor suitable for testing single-bead catalysts in a highly parallel fashion, the so-called “*single-bead reactor*,” is designed as a two-dimensional arrangement of *microreaction chambers* which can each hold one *catalytic bead*. The reactor can be divided into two parts, a base part and a top part. The base part is filled with beads, and the top part is then pressed, sealed, or bonded against the base part to encapsulate each bead in a single independent microreaction chamber. The beads sit loosely in the reaction chambers, allowing continuous fluid flow from openings in the top part of the reactor, around the bead, and through openings in the base part. To avoid mass transfer problems while reacting the fluid on the bead, eggshell-type catalytic beads can be used.

Using the top-down direction as fluid flow path and the small footprint of a single microreaction chamber allows extension of the reactor in two dimensions. This is not possible using microchannel-based approaches, as the microchannels extend as straight long channels on a substrate and therefore block one dimension [26]. In most cases parallel microchannel reactors on a substrate are one-dimensional arrangements of channels, having a much larger footprint than a two-dimensional arrangement of reaction chambers such





as the single-bead reactor. The resulting *array density* is much higher for the single-bead reactor, reaching up to 60 or more catalytic reaction chambers per square centimeter [37].

### Reactant Distribution Options for Miniaturized Reactors

In order to carry out comparable catalytic experiments in a high-throughput parallel mode, *equal reaction conditions* for each library member have to be ensured. This is especially true for *reactant distribution*, as variations in residence time and space velocity can have a dramatic impact on the performance.

For conventional laboratory reactors, reactant flow is usually controlled by mass flow controllers that use valves to adjust the pressure drop for the fluid flow through the controller, thus regulating mass flow. Such an active control of fluid flow for each reaction chamber would probably not be possible, for reactors with several hundred parallel reaction chambers, or at least would not be economic as long as there are no dramatic developments and improvements in micro electro-mechanical systems (MEMS) devices.

Adjusting the *pressure drop* along the *fluid flow path* is the key to controlling the fluid flow rate [38]. This also holds true for passive control of pressure drop by geometric design of the flow path. In contrast with active control elements, passive *flow restrictors* like capillaries or orifices can already be miniaturized and tightly integrated into a microreactor design.

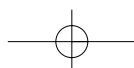
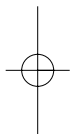
An approach using capillary *manifolds* or microchannel manifolds, known as “binary trees,” has been described by Bergh and Guan [25], among others. A channel network is built onto a flat wafer substrate that splits a common feed channel recursively into two new feed channels. As a result, a tree of splitting channels is generated which connects 256 reaction chambers with the common feed channel (Figure 23.1). The channel length and channel geometry to each of the chambers is the same, resulting in an equal pressure drop and therefore an equal reactant distribution. However, the channel network is very complex, and all reaction chambers are connected by the network. These interconnections may present a considerable limitation. For instance, a single particle in the feed stream may clog and block a whole subtree of the channel network. Furthermore, the tree becomes increasingly complex with increasing number of reaction chambers, therefore limiting *scalability*. Finally, the channel network occupies a considerable amount of space on the wafer, limiting the density of the reaction chambers.

As presented, there may be a number of drawbacks resulting from the single fact that the channels, that is, the flow restrictors causing pressure drop, are connected to each other. However, if we consider only the required pressure drop, there is no need to connect all the channels in a tree format.

An obvious solution to this problem is to use single independent flow restrictors for each reaction chamber. In an early design study, the pressure drop of fluid flow through short narrow channels or pores was calculated using the Hagen–Poiseuille law:

$$\Delta p = \frac{8}{\pi} l_p \dot{V}_B \eta \frac{1}{r_p^4 N} \quad (1)$$

with  $l_p$  is the pore length,  $\dot{V}_B$  is the flow rate,  $\eta$  is the viscosity,  $r_p$  is the pore radius, and  $N$  is the pore number.



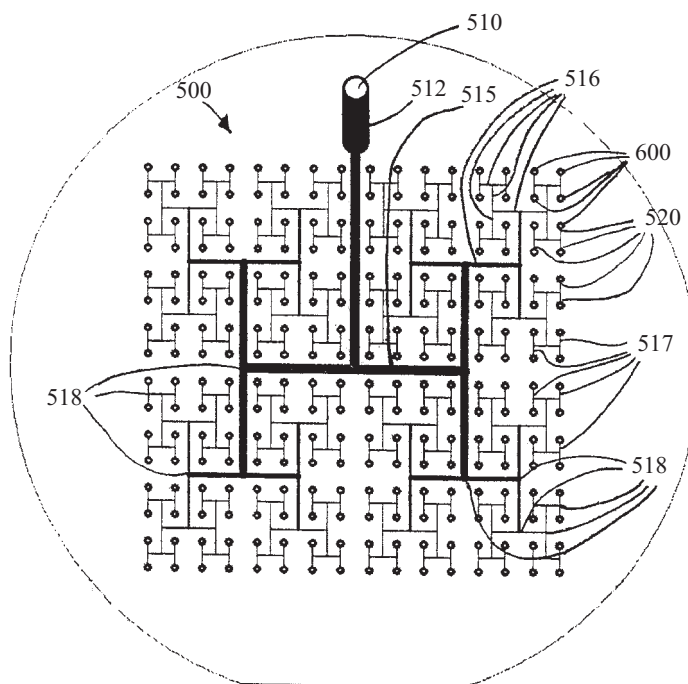
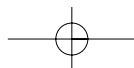


FIGURE 23.1. Reactant distribution using a binary-tree channel network [25].

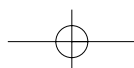
As can be seen in Figure 23.2, a considerable pressure drop can be generated depending on the pore number and the pore radius. In particular, small pore radii result in a strong increase in the pressure drop. From this rough calculation, it is clear that such arrangements of short narrow pores can be sufficient to generate an equal flow distribution.

Therefore the fluid access ports of the microreaction chambers have been designed as flow restrictors in our “single-bead approach.” These flow restrictors are *microstructured membranes* comprising a collection of a defined number of short straight pores with a very small diameter, as described below.

### Computational Fluid Dynamics Calculations

The development of miniaturized reactors is supported by CFD calculations. We used CFD to study several crucial items of the design of the high-throughput reactor: (1) the realization of uniform inlet flow conditions in individual microreaction chambers, (2) the spatial profiles of the pressure, velocity, temperature, and species concentrations inside these chambers, and (3) potential interference of the microreaction chambers, mainly by thermal conductivity. The first two items will be discussed in more detail in this section.

The CFD *simulation* of our reactor is based on the solution of the steady state three-dimensional *Navier–Stokes* equations for gaseous flows. The flow fields are always laminar due to the small reactor sizes. A mass source term, gravitational and external body



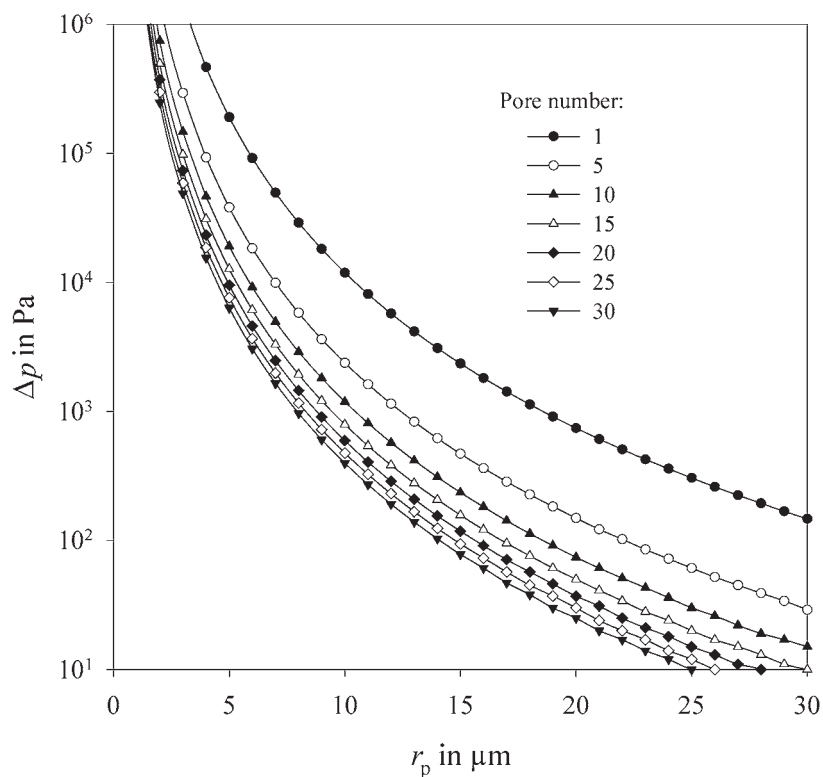


FIGURE 23.2. Pressure drop for fluid flow through short narrow pores as function of pore radius and pore number:  $l_p = 100 \mu\text{m}$ ,  $\dot{V}_B = 1 \text{ ml min}^{-1}$ ,  $\eta = 28 \mu\text{Pa s}$ .

forces, thermal diffusion, viscous heating, and homogeneous chemical reactions in the gas phase are not significant in the reactor. We do not consider the thermal interference between different reactor chambers, which will be described in a future publication, but assume an isothermal reactor. This results in the following system of conservation equations.

Continuity:

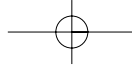
$$\frac{\partial(\rho v_j)}{\partial x_j} = 0 \quad (2)$$

Momentum:

$$\frac{\partial(\rho v_j v_i)}{\partial x_j} + \frac{\partial p}{\partial x_i} - \frac{\partial \tau_{ij}}{\partial x_j} = 0 \quad (3)$$

with stress given by

$$\tau_{ij} = \mu \left( \frac{\partial v_i}{\partial x_j} + \frac{\partial v_j}{\partial x_i} - \frac{2}{3} \delta_{i,j} \frac{\partial v_k}{\partial x_k} \right)$$



Species mass:

$$\frac{\partial(\rho v_j Y_i)}{\partial x_j} + \frac{\partial j_{i,j}}{\partial x_j} = 0 \quad (i = 1, \dots, N_g) \quad (4)$$

with the diffusion mass flux in the  $x_j$  direction given by

$$j_{i,j} = -\rho D_i^M \frac{\partial Y_i}{\partial x_j}$$

In the above equations, the  $x_j$  ( $j = 1, 2, 3$ ) are cartesian coordinates,  $v_j$  is the cartesian component of the velocity vector,  $\rho$  is the mass density,  $p$  is the pressure,  $Y_i$  is the mass fraction of species  $i$  in the mixture,  $N_g$  is the number of gas phase species, and  $D_i^M$  is the effective diffusion coefficient of species  $i$  into the mixture. The transport properties, viscosity  $\mu$  and diffusion coefficients  $D_i^M$ , depend on temperature and composition [39,40]. The Einstein convention is used; that is, whenever the same index appears twice in any term, summation over that index is implied, except if the index refers to a chemical species. The system is closed by the equation of state

$$p = \frac{\rho RT}{\bar{M}} \quad (5)$$

where  $T$  is temperature,  $R$  is the universal gas constant, and  $\bar{M}$  is the mean molar mass of the mixture.

On the reactive surface of the catalytic bead the following boundary conditions are used for the species continuity equation:

$$\mathbf{n} \cdot \mathbf{j}_i = \dot{s}_i \bar{M} F_{\text{cat/geo}} \quad (i = 1, \dots, N_g) \quad (6)$$

where  $\mathbf{n}$  is the outward-pointing unit vector normal to the surface,  $\dot{s}_i$  are the chemical reaction rates due to heterogeneous reactions at the catalytic surface, and  $F_{\text{cat/geo}}$  is the ratio of catalytic active surface area to geometric surface area. No-slip boundary conditions are chosen for the momentum equation at all solid surfaces; that is, all velocity components vanish at the gas–surface interface.

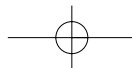
The molar net production rate  $\dot{s}_i$  of a gas phase species or an adsorbed species due to heterogeneous reactions on the solid surface is then given by

$$\dot{s}_i = \sum_{k=1}^{K_s} \nu_{ik} k_{fk} \prod_{i=1}^{N_g + N_s} c_i^{\nu'_{ik}} \quad (i = 1, \dots, N_g + N_s) \quad (7)$$

where  $K_s$  is the number of surface reactions,  $\nu_{ik}$  and  $\nu'_{ik}$  are stoichiometric coefficients,  $k_{fk}$  is the rate coefficient of reaction  $k$ ,  $c_i$  are species concentrations, and  $N_s$  is the number of adsorbed species. For complex heterogeneous reactions the expression for the rate coefficient  $k_{fk}$  can become rather complex:

$$k_{fk} = A_k T^{\beta_k} \exp\left(\frac{-E_{ak}}{RT}\right) \prod_{i=1}^{N_s} \theta_i^{\mu_{ik}} \exp\left(\frac{\epsilon_{ik} \theta_i}{RT}\right) \quad (8)$$

where  $A_k$ ,  $\beta_k$ , and  $E_{ak}$  are the pre-exponential factor, the temperature exponent, and the activation energy, respectively, for reaction  $k$ . The parameters  $\mu_{ik}$  and  $\epsilon_{ik}$  describe the dependence of the rate coefficients on the surface coverages  $\theta_i$  of species  $i$  [29,41,42].



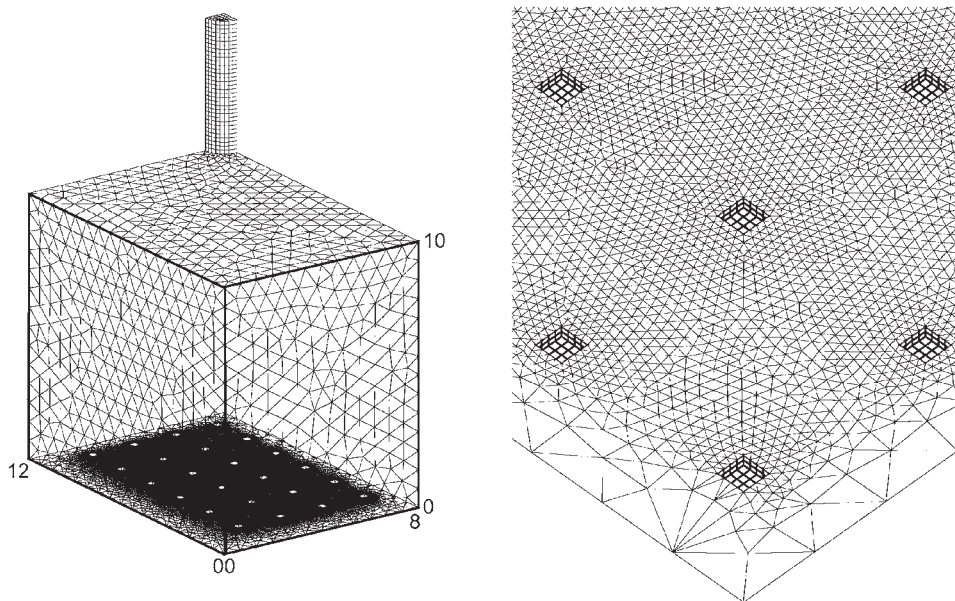
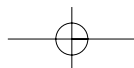


FIGURE 23.3. Computational grid at the walls of the reactor (left) and at the outlets (right) (scales in millimeters).

The numerical simulation is based on the commercial finite-volume CFD code Fluent [43], which was coupled with our software package DETCHEM [42] for simulation of the chemical reactions.

First, CFD was used to ensure an even flow distribution over the microreaction chambers; that is, each reactor is loaded with the same mass flow. Therefore the flow field distribution in the reactor head and its inlet and outlets was calculated. The reactor geometry is as follows. The premixed reactants flow through a tube 1.6 mm in diameter and 5 mm long that enters the reactor head in the center. Owing to symmetry, only a quarter of the reactor head needed to be analyzed (Figure 23.3). The transition from the reactor head to a single-bead reactor with 96 microreaction chambers is achieved by membranes at the entrance to the reactor.

The grid generator GAMBIT [43] was used to construct an *unstructured grid*. Since the sizes of the reactor head and the membranes differ tremendously, approximately 200,000 vertices were needed to produce a computational grid that leads to a converged solution. This grid is shown in Figure 23.3.

Since the reactants are premixed and no reactions occur in the reactor head, the species mass equations are not solved. The membranes are modeled by the *porous media model*, which is provided by the CFD code Fluent [43]. The membranes consist of sets of thin vertical channels. The pressure drop over these membranes can be estimated by applying the Hagen–Poiseuille law and then used to derive the parameters internal resistivity and permeability for Fluent’s porous media model [43]. Since the pressure drop is also predicted by the CFD code, this value can be used as an additional empirical convergence check.

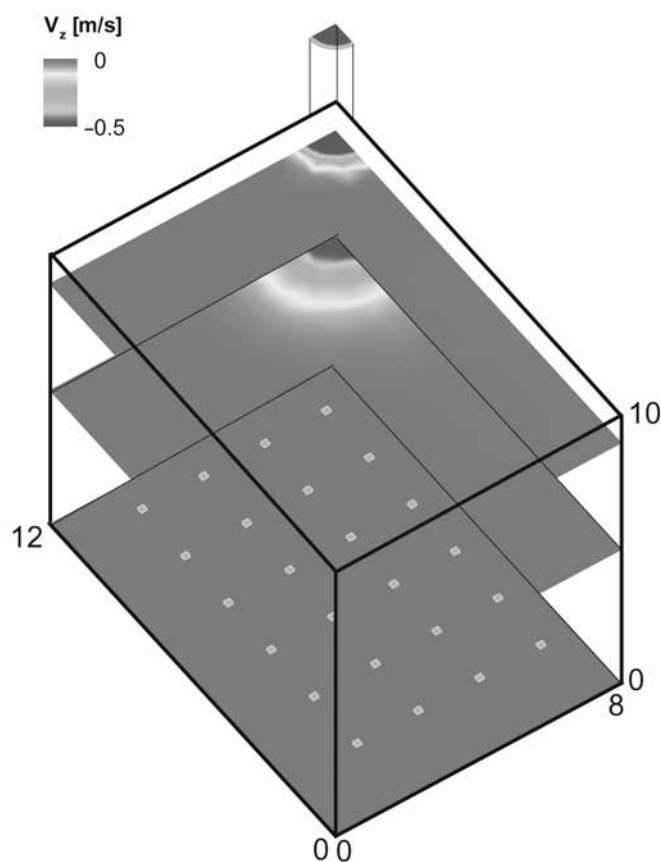


FIGURE 23.4. Vertical velocity at different horizontal planes in the reactor head (scales in millimeters). The actual minimum velocity is  $-1.4 \text{ m s}^{-1}$ .

As expected, the simulation revealed that under the given conditions, and also within a wide range around those conditions (e.g., reactor geometry, membrane parameters, flow rate), the mass flow through all the membranes is the same. The maximum deviation from the mean value is less than 0.01%, which is within the numerical error. Figure 23.4 illustrates this fact by showing the vertical flow velocity for different levels inside the reactor head. It should be noted that the levels are shown in reverse order to give a better view of the interesting lowest level, where the fluid inlets to the reaction chambers are located.

The second point of interest was the description of the reactive flow field inside the microreaction chamber shown in Figure 23.9. The simulation is carried out for the region between wafers 2 and 4, that is, from the top of the inlet membrane to the bottom of the outlet membrane. The membranes are again treated as porous media. The heterogeneous reactions occur on the spherical bead inside the reaction chamber consisting of rectangular pyramid sections below the inlet and above the outlet membrane and in the cylindrical middle part. The bead diameter was varied in the simulation. Because of symmetry, only an eighth of the reactor needs to be simulated. Nevertheless 20,000 vertices forming

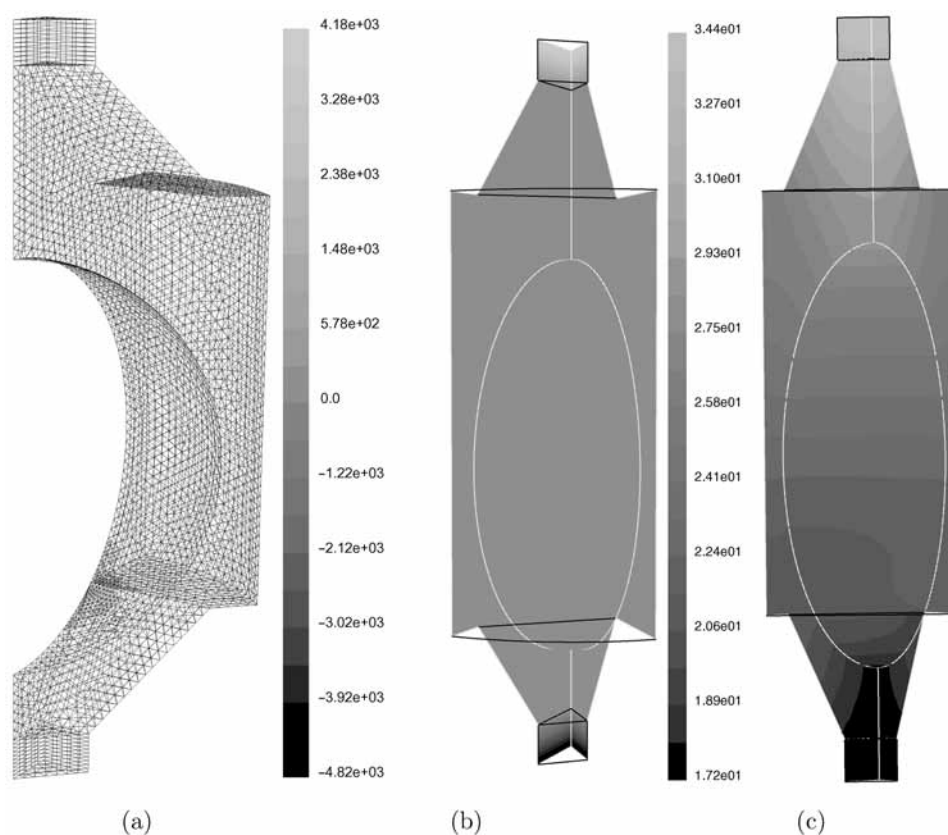


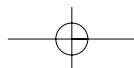
FIGURE 23.5. (a) Computational grid of the simulated section (one eighth) of the microreaction chamber. Only knots on the bead, reactor, and section walls are shown. (b) The calculated pressure drop (Pa) and (c) the CO mass fraction inside the microreaction chamber.

80,000 cells were generated using GAMBIT [43]. Lower spatial resolution did not lead to successfully converged solutions. As an example, the computational grid generated for a reactor with a bead of diameter 1 mm is shown in Figure 23.5(a).

The catalytic formation of butane from synthesis gas (CO and hydrogen) serves as an example reaction. The kinetics was arbitrarily set to first order in hydrogen and CO.

In the example discussed, the rate coefficient was set to a value of  $10^{-2} \text{ m}^6 \text{ mol}^{-1} \text{ s}^{-1}$  which ensures almost complete conversion. Under these conditions, a potential *transport limitation* would be most significant. The initial composition (mass fractions) is given as 0.344, 0.056, and 0.60 for CO, hydrogen, and argon, respectively. An *isothermal reactor* of 400 K was assumed, even though the reaction will release significant heat. The heat distribution in microreactors for high-throughput screening has also been studied and will be discussed in a future publication.

Figures 23.5(b) and 23.5(c) show the numerically predicted pressure drop and CO mass fraction for a bead with a diameter of 1 mm. The pressure drop in the reactor occurs almost exclusively over the two membranes; this also holds for larger beads. Strong



vertical gradients of the CO concentration occur under the chosen conditions (high conversion). The single reaction chamber is far from being ideally mixed. Rather, it resembles a *plug-flow reactor*.

We have shown that CFD calculations can assist in the design of miniaturized reactors for high-throughput techniques. Different reactor concepts and varying reactor parameters and conditions can be tested much faster by using computational tools than by constructing a new reactor. For the concept discussed here, CFD simulations confirmed the even flow distribution over the single reaction chambers and revealed the processes inside the single-bead reactor. Since these were three-dimensional configurations and varying length scales, a complex computational grid had to be constructed, necessitating a very large computing effort when using complex kinetics.

### Layout and Manufacture

The cross-section of a simple single-bead reactor layout is depicted in Figure 23.6. Wafers 1 and 2 are bonded together and represent the base part of the reactor; wafer 3 is the top part. The silicon wafers are structured by wet etching procedures such that microreaction chambers are formed the top and bottom parts are pressed together. These microreaction chambers consist of a cuboid and two frustums of a pyramid. Microstructured membranes are fabricated at the top and the bottom of the reaction chambers by deep reactive ion etching. One reaction chamber has an internal volume of approximately  $0.8 \text{ mm}^3$  and can hold a single *catalytic bead*. Beads of different sizes can be used; however, in this simple setup, no measures were taken to fix the position of the bead in the center of the reaction chamber.

Figure 23.7 shows the corresponding top view of the base part of such a reactor: A total of 105 reaction chambers were fabricated as a  $15 \times 7$  arrangement on a very small reactor footprint. Excluding the outer margins used for sealing, the array density is approximately 60 reaction chambers per square centimeter.

A number of scanning electron microscope (SEM) of the microreaction chambers of this reactor type are shown in Figure 23.8. The dense arrangement of the chambers is obvious [Figure 23.8(a)]. The structure of the microreaction chambers of the base part can

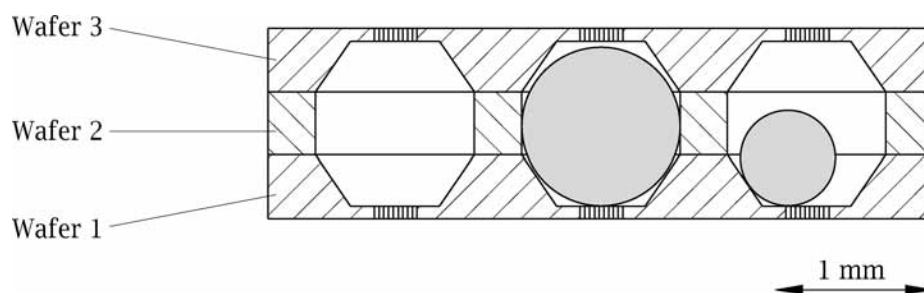
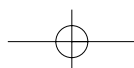


FIGURE 23.6. Partial cross-section of a simple single-bead reactor, showing three microreaction chambers without beads and with beads of different sizes in the reaction chambers.



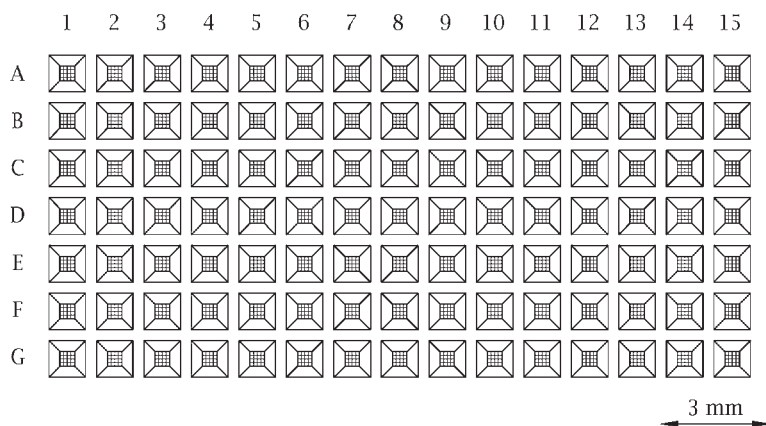
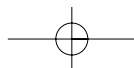


FIGURE 23.7. Top view of a simple 105-parallel single-bead reactor array. The positions of the reaction chambers are indicated.

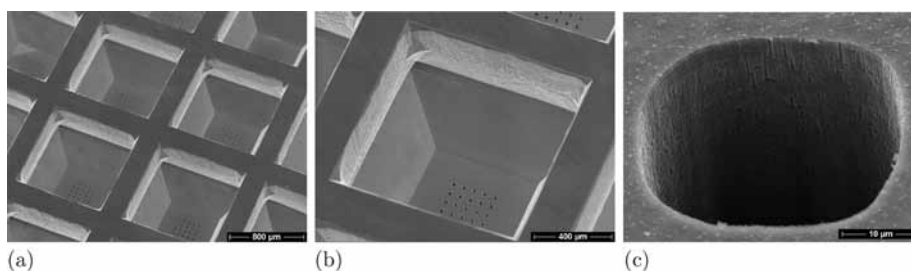
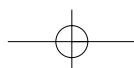


FIGURE 23.8. Scanning electron microscope (SEM) pictures illustrating the structure of a single-bead reactor consisting of a base part and a top part: (a), (b) reaction chambers in the base part; (c) single pore of a pore membrane.

be seen in Figure 23.8(b) as a stack of a cuboid and a frustum of a pyramid. The entrance to a single pore of a membrane is shown in Figure 23.8(c).

The partial cross-section of an advanced single-bead reactor is shown in Figure 23.9. The complete setup consists of four wafers, where wafers 1–3 form the base part of the reactor and wafer 4 forms the top part. The microreaction chambers are larger than in the simple setup and contain means for fixing the position of the bead. A number of possible designs can be envisaged; however, a simple frustum of a pyramid was chosen for compatibility with the well-known wet etching processes. Another advantage of the pyramid is its tolerance to variations in the size and form of the beads. A spherical bead cannot block the quadratic cross-section of the frustum. Furthermore, different bead sizes can be employed; however, the bead size is usually kept constant during an experiment. In addition, the beads are not in contact with the pore membranes.

Wafers 2 and 4 are processed identically to reduce fabrication costs. The additional wafer 1 contains a product withdrawal zone, which can be used for sampling with a narrow



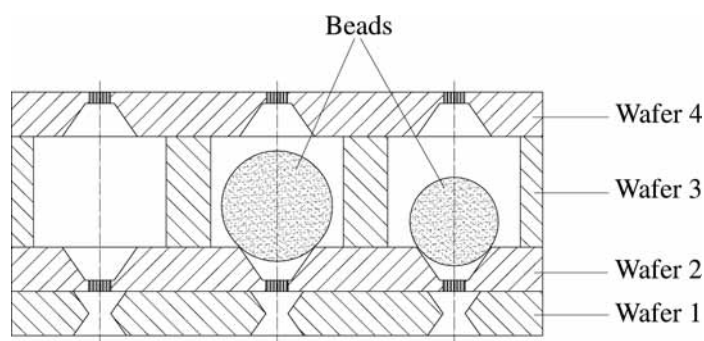
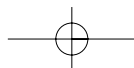


FIGURE 23.9. Advanced configuration of a single-bead reactor shown in partial cross-section with and without beads in the reaction chambers.

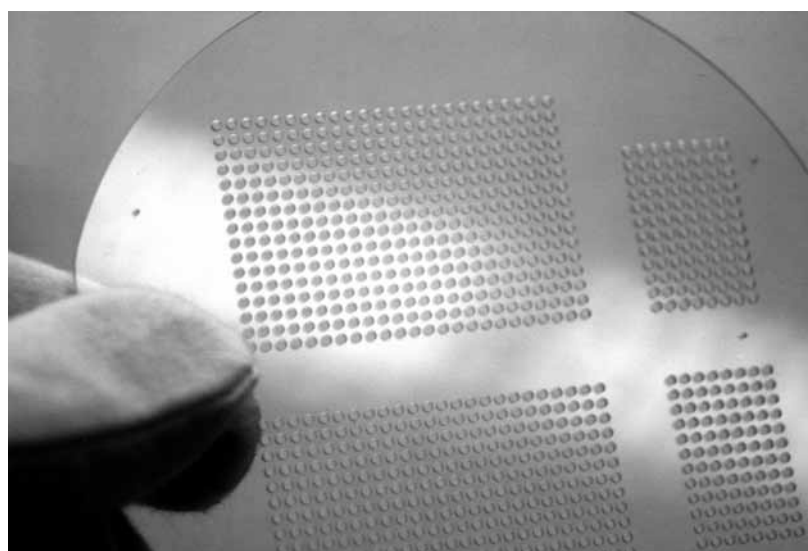
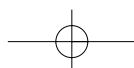


FIGURE 23.10. An ultrasonically micromachined Pyrex wafer forming part of the single-bead reactor. Two 384-parallel arrays and two 96-parallel arrays can be prepared on a single 100 mm Pyrex substrate.

*capillary* in order to allow a fast *sequential analysis*. Wafer 1 can be bonded to wafer 2 by suitable *bonding* technologies.

While standard *silicon* wafers with a thickness of 200–800  $\mu\text{m}$  can be used for wafers 1, 2 and 4, wafer 3 is usually thicker and has cylindrical holes to increase the height of the reaction chambers. Therefore wafer 3 was constructed from Pyrex and the holes were fabricated by parallel ultrasonic drilling. A structured Pyrex wafer is shown in Figure 23.10. Two 384-parallel arrays as well as two 96-parallel arrays can be fabricated on a 100 mm substrate, illustrating once again the high *array density* of the single-bead approach. Photographs of the fabricated arrays of 105 and 384 parallel reactors are shown in Figure 23.11.



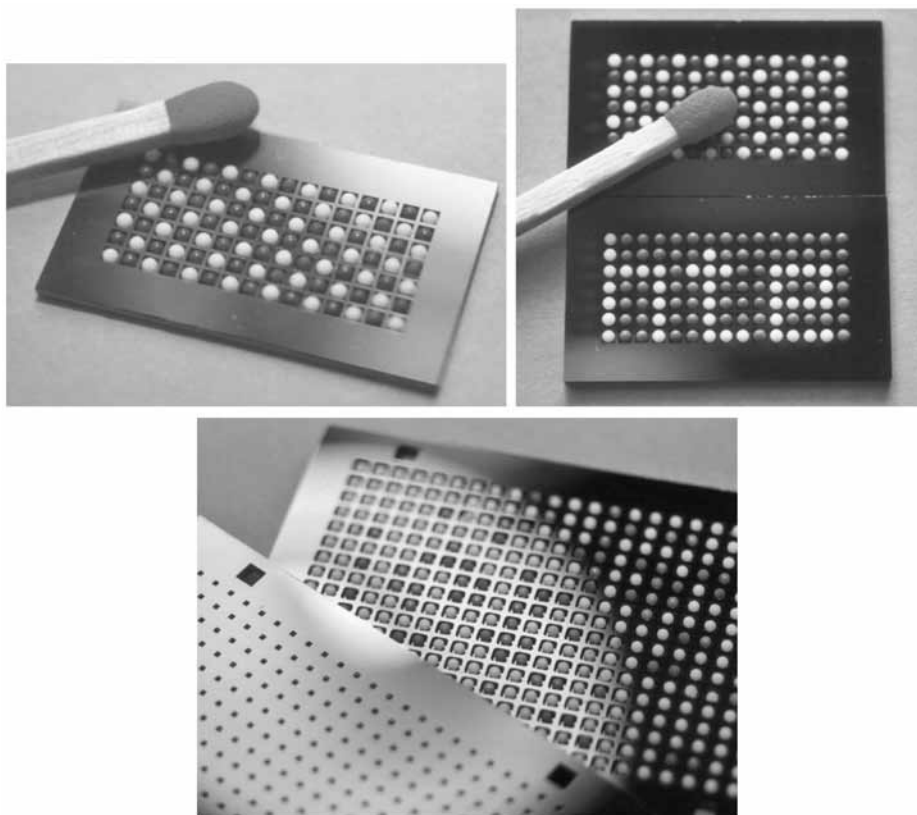
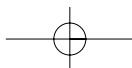
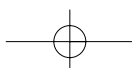


FIGURE 23.11. View of different 105-parallel and 384-parallel single-bead reactors.

## Application and Results

Several sets of experiments were carried out to evaluate the performance of the different single-bead reactors in *continuous flow* catalytic experiments. Beads of 2% Pd- $\gamma$ -Al<sub>2</sub>O<sub>3</sub> with a diameter of 1 mm were prepared from  $\gamma$ -Al<sub>2</sub>O<sub>3</sub> by wet impregnation and subsequent calcination at 450°C. The mass of one catalytic bead was approximately 700  $\mu$ g.

Such Palladium catalysts are known to be active in hydrogenation reactions. Together with inactive reference beads, a 105-parallel single-bead reactor was charged as shown in Figure 23.12 and tested in the *partial hydrogenation* of 1,3-butadiene at 60°C. The base and top were pressed together using a suitable heatable flange system and mounted into a test rig. The reactants were continuously supplied by mass flow controllers and preheated to the reaction temperature before entering the reactor. The product analysis was carried out in a fast sequential mode by *spatially resolved mass spectrometry*, as described in detail later in this chapter. Figure 23.13 shows a section of the reactor base together with the *sampling capillary* in front of a specific product outlet.



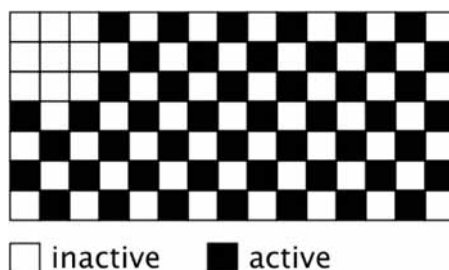
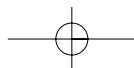


FIGURE 23.12. Arrangement of catalysts in a single-bead reactor for the validation of the reactor system: inactive catalyst, pure  $\gamma$ - $\text{Al}_2\text{O}_3$  beads; active catalyst, 2% Pd- $\gamma$ - $\text{Al}_2\text{O}_3$  beads.

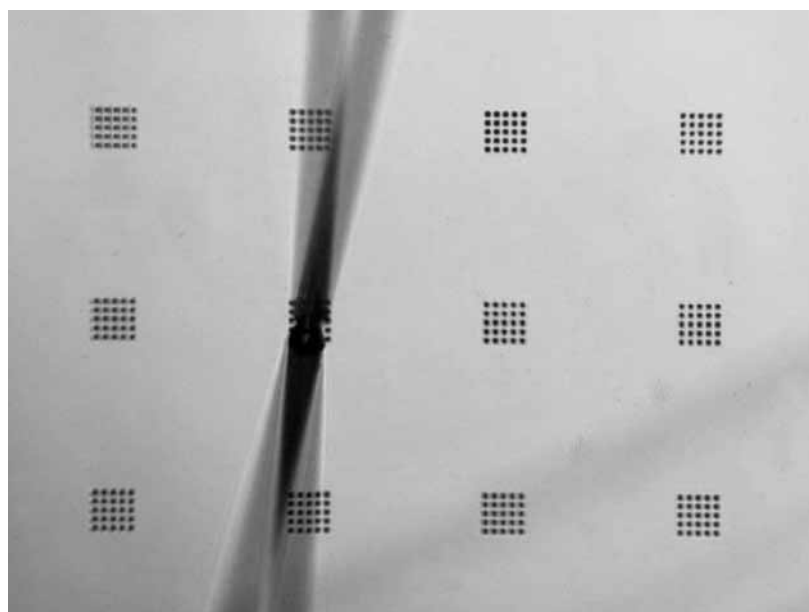
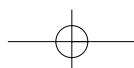


FIGURE 23.13. Product outlets in the base of the 105-parallel single-bead reactor and the capillary probe in front of a product outlet.

An example of the results of a screening are shown in Figure 23.14. At a residence time of about 10 ms, conversion degrees of approximately 50% are achieved on the active catalysts [Figure 23.14(a)]. In contrast, only very low conversions are measured for the inactive samples. This indicates that the *cross talk* between adjacent members of the library is almost negligible. Furthermore, only slight differences in the cumulative selectivities to the *n*-butenes are measured [Figure 23.14(b)].

The results for a residence time  $\tau$  of 32.5 ms are shown in Figure 23.14(c). Compared with  $\tau = 10.8$  ms, the resulting conversion degrees for the active catalysts are higher, but the conversion for the inactive reference catalysts is still very low. Nevertheless, a slight trend in the conversion degree from position B15 to F1 can be observed for both residence times. As identical Palladium catalysts from the same preparation batch were used, this trend is believed to arise from the reactor configuration. To exclude a potential reactant



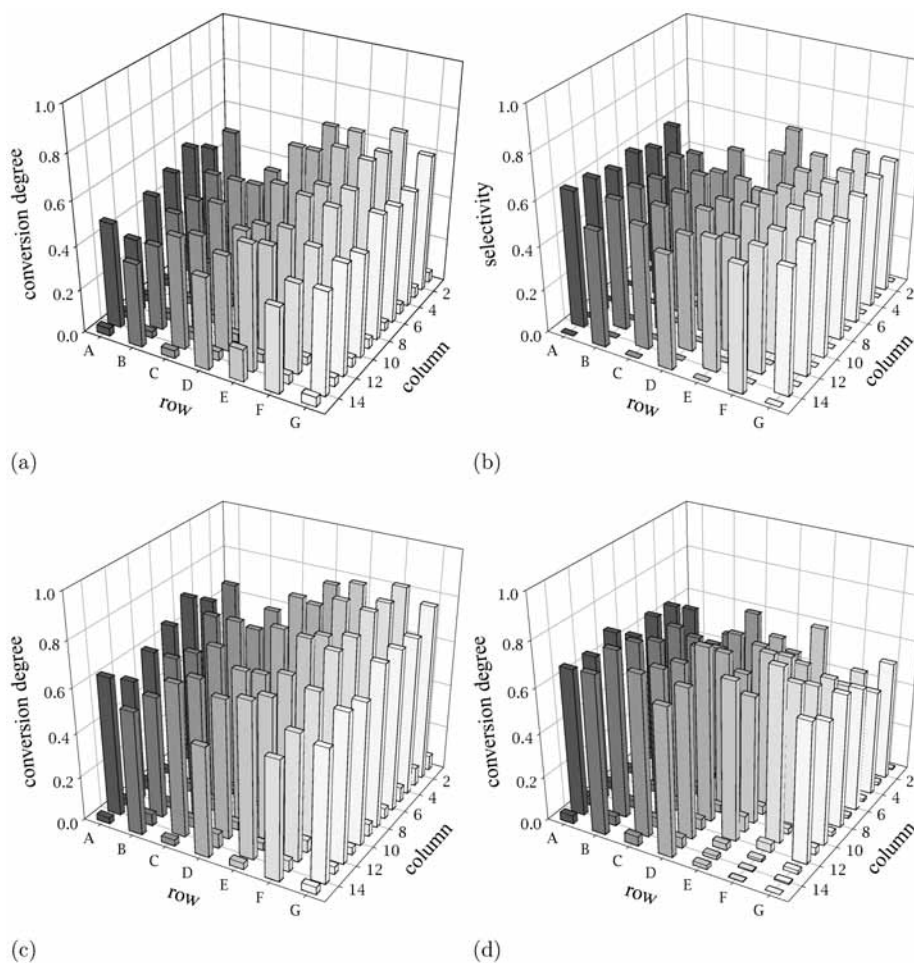
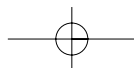
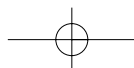


FIGURE 23.14. (a) Results from the high-throughput screening of identically prepared 2% Pd- $\gamma$ -Al<sub>2</sub>O<sub>3</sub> beads and inactive  $\gamma$ -Al<sub>2</sub>O<sub>3</sub> beads in the partial hydrogenation of 1,3-butadiene. Reaction conditions:  $T_R = 60^\circ\text{C}$ , 3 vol.% C<sub>4</sub>H<sub>6</sub>; 3 vol.% hydrogen; balance, argon. (a) Conversion degree,  $\tau = 10.8$  ms. (b) Cumulative selectivity to *n*-butenes,  $\tau = 10.8$  ms. (c) Conversion degree,  $\tau = 32.5$  ms. (d) Conversion degree,  $\tau = 10.8$  ms, reactor rotated by 180°.

*maldistribution* induced by the flange or the heating system, the library was rotated by 180° and the experiment was repeated under the same reaction conditions ( $\tau = 10.8$  ms). The results are shown in Figure 23.14(d). Again, a trend in the conversion is observed, but now in the opposite direction.

The reason for this trend was identified by measuring the pore sizes of the single pores of the membranes across the reactor (Table 23.1). As can be seen, there are rather large deviations in the pore size and the resulting pore area, which determines the resistance to fluid flow. The pores in column 15 of the reactor are considerably larger than the pores in column 1. This means that the resistance to flow is higher column 1, which leads to a maldistribution of reactants with lower flow rates and thus higher residence times per



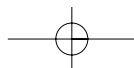


TABLE 23.1 Variation in Pore Size in the 105-Parallel Single-Bead Reactor

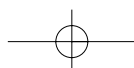
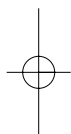
	Position	$a_{\min}$	$a_{\max}$	$b_{\min}$	$b_{\max}$	$A_{\text{pore}}$	$\Delta A_{\text{pore}}$
Base	A 1	0.92	0.96	1.00	1.08	0.98	-0.02
	G 1	1.02	1.08	0.96	1.12	1.09	0.09
	A 15	1.08	1.15	1.08	1.19	1.27	0.27
	G 15	1.05	1.15	1.00	1.15	1.19	0.19
Top	A 1	0.89	0.92	0.85	0.96	0.82	-0.18
	F 1	0.86	0.92	0.85	0.92	0.79	-0.21
	G 1	0.86	0.92	0.85	0.85	0.76	-0.24
	A 15	1.02	1.04	0.96	1.12	1.07	0.07
	B 15	1.02	1.08	1.04	1.12	1.13	0.13
	G 15	0.95	1.08	0.96	0.96	0.98	-0.02

reaction chamber in column 1. As indicated by the results shown in Figures 23.14(a) and 23.14(c), longer residence times lead to an increase in conversion. Thus the observed trend in the conversion degree from one region of the reactor to another can be explained by the differences in the pore sizes of the pore membranes. Finally, we determined that the pore size differences resulted from the use of an inexpensive emulsion mask process for fabricating the pore membranes.

A major improvement in terms of flow distribution could be achieved by the more accurate fabrication process that was used to develop *384-parallel single-bead reactors* with a  $24 \times 16$  format. Before using this reactor in catalytic reactions, the pore sizes were determined by optical microscopy. The pore size distribution (Figure 23.15) indicates excellent pore uniformity.

As an example, the 384-parallel single-bead reactor was applied in a *partial oxidation* reaction. In an initial experiment, the reactor was filled with inactive and active catalysts according to the pattern shown in Figure 23.16(a). A continuous flow screening experiment was carried out at  $400^\circ\text{C}$  and a reactant flow  $\dot{V}$  of  $1 \text{ ml min}^{-1}$  per bead, again using spatially resolved mass spectrometry for *sequential product analysis*. The normalized results for the conversion degree are shown in Figure 23.16(b). According to the mass spectrometric intensities, white colors represent low conversions of the hydrocarbon and dark colors represent high conversions. The maximum conversion in this experiment is approximately 60%. As can be seen, the results for the conversion degree are in good agreement with the filling pattern of the reactor. *Cross talk* between adjacent reaction chambers can be observed to some minor extent, although it does not limit the applicability of the single-bead reactor for primary screening purposes. Furthermore, it is expected that cross talk can be reduced by bonding the base and the top of the reactor, instead of just pressing them together as presented here.

It can be concluded that the single-bead reactor concept provides a novel system architecture for the high-throughput primary screening of *solid catalysts*. By using single beads as catalytic materials and a *scalable* method for the fluid distribution, array densities of up to 60 catalysts per square centimeter have successfully been applied. This array density vastly exceeds those used by other groups. Thus it is possible to realize parallel reactors for heterogeneous catalysis with a much higher degree of parallelization as shown successfully with the 384-parallel single-bead reactor.



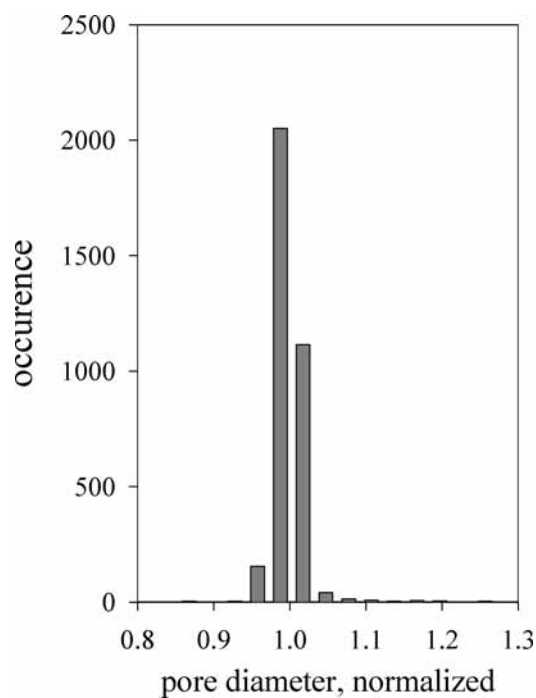


FIGURE 23.15. Pore size distribution of pore membranes prepared by a deep reactive ion etching process on a silicon wafer.

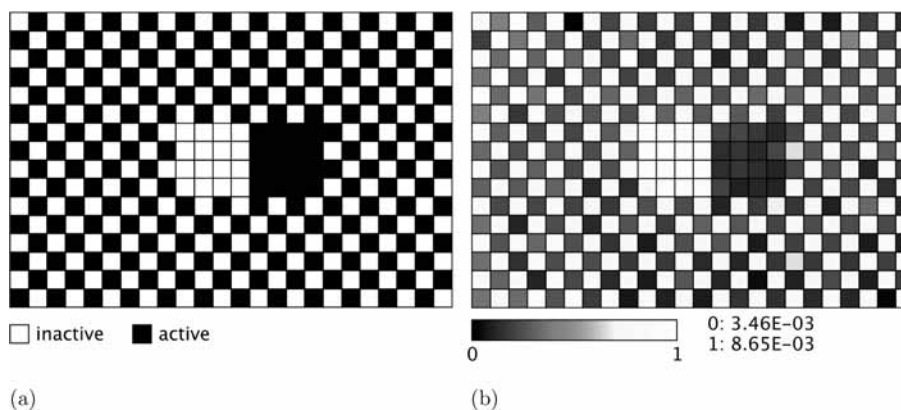
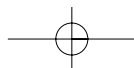


FIGURE 23.16. Results of high-throughput screening of catalysts in a 384-parallel single-bead reactor in a partial oxidation reaction: (a) arrangement of inactive and total oxidation catalysts in the reactor; (b) screening results for the conversion of a hydrocarbon at 400°C and a reactant flow of 1 ml min<sup>-1</sup> per bead.

The *multifunctional reactor* architecture developed enables *handling*, *identification*, and *storage* of the catalysts, and the *automation* and *integration* of the complete *high-throughput workflow*. This includes the possibility of adapting different sequential or parallel analysis techniques for the detection of interesting products. The versatility of the



system facilitates its application to different classes of reaction. Operation at conditions relatively close to conventional and/or secondary catalyst test systems can be ensured.

### Novel Preparation Techniques for the Single-Bead Reactor Concept

As a consequence of the increasing parallelization and integration of reactor systems, requirements for synthesis methodologies are becoming more extreme. The synthesis of minute amounts of material (i.e., different multicomponent mixed oxides in the microgram or milligram range) must be reproducible and fully automated. Meeting these challenges demands a combination of different expert skills in inorganic synthesis, robotics, automation, and related fields.

Related to the previously unmet degree of parallelization possible with the single-bead reactor concept, new methods are needed to avoid bottlenecks in the preparation of the catalyst libraries. Of course, it may be possible to apply highly parallel preparation methods for single beads (e.g., by suitable micropipetting robots) where each bead is placed in a separate well on a synthesis platform. However, the resources needed to install such a work flow scale at least linearly with the number of beads to be prepared in a given timeframe. Furthermore, only simple catalyst preparation methods like wet impregnation seem to be manageable on such a small scale.

Several strategies for the preparation of large diverse molecular libraries are well known in combinatorial approaches in organic and bio-chemistry. One of the most powerful concepts for the generation of very large libraries is the so-called “*Split & Pool*” technique [44,45] (Figure 23.17). This technique provides an efficient strategy for assembling

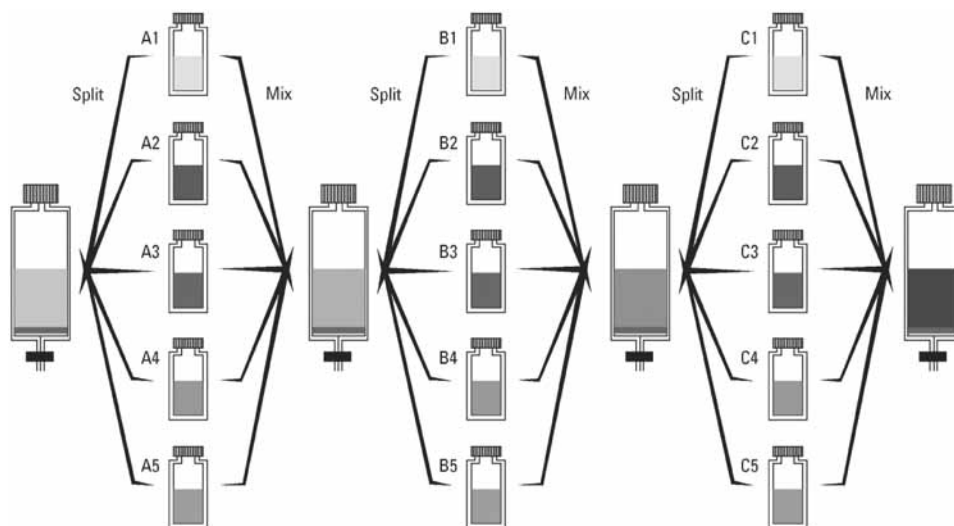
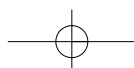


FIGURE 23.17. Principle of the Split&Pool method [52].



combinatorial libraries. The solid support is divided into portions, each of which undergoes a reaction with a single building block. Pooling of these portions results in a single batch of solid support bearing a mixture of components. Repetition of the *divide*, *couple*, and *recombine* processes results in a library where each discrete particle of solid support carries a single library member, and the number of members is equal to the product of the number of building blocks incorporated at each step.

Furthermore, libraries prepared by Split & Pool are fully combinatorial libraries containing all possible combinations of building blocks. Therefore it is possible to produce highly diverse libraries containing  $10^4$ – $10^8$  samples with a very simple work flow.

Using single beads as basis of the single-bead reactor concept enables us to adopt equivalent strategies for the preparation of inorganic material libraries, even if the preparation of such libraries presents different challenges than those encountered in the organic realm so that a self-contained independent methodology is required. For instance, if wet impregnation is used as preparation method, the percentage loading of a support has to be controlled precisely, the resulting elemental distributions have to be controlled, and other factors involving the solid state materials have to be taken into consideration. Furthermore, the application of such *pooled synthesis* techniques in inorganic chemistry reaches far beyond the elemental/compositional diversity known from Split & Pool for molecular entities. In inorganic chemistry, the *diversity parameters* include not only compositions but also *precursors*, *supports*, *pre- and post-treatment*, etc.

Split & Pool, perhaps carried out via special routes such as “*directed sorting*” [47,48] or “*direct divide*” [49], provides a very powerful method for generating diverse libraries of inorganic materials. An example of part of a library is shown in Figure 23.18.

Further prospects, implications, and results from the application of this method for combinatorial material science are published elsewhere [50].

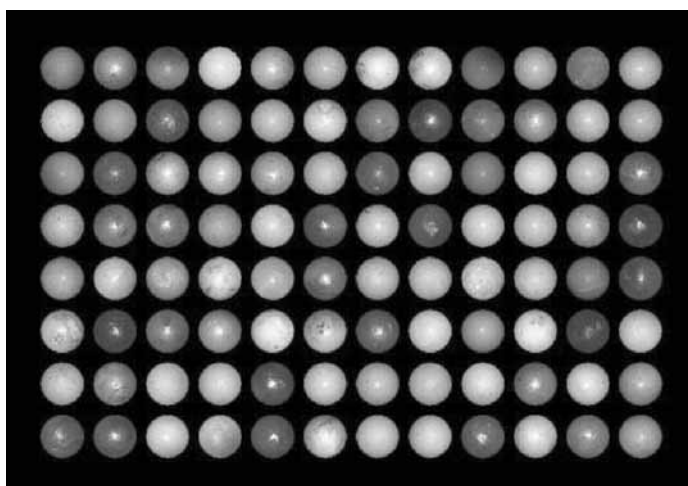


FIGURE 23.18. A 96-parallel single-bead reactor filled with beads prepared by inorganic Split & Pool.

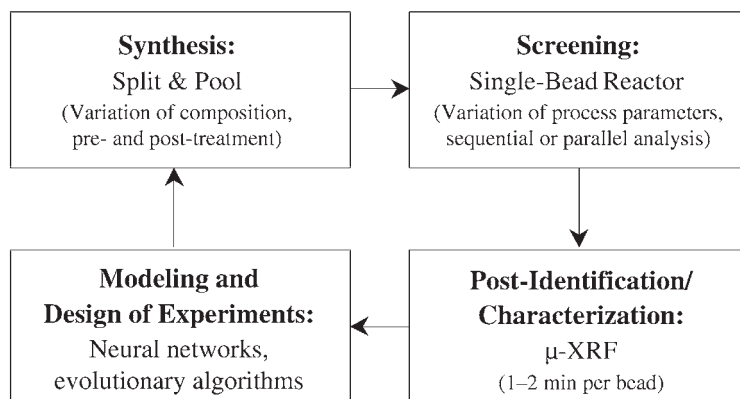
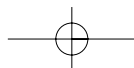


FIGURE 23.19. Simplified work flow for primary screening in heterogeneous catalysis applying the “single-bead” concept.

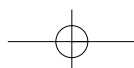
### Work Flow for the Screening of Bead Catalysts

To avoid bottlenecks in the screening work flow, the different elements of a high-throughput research program, especially in primary screening, need to be tightly integrated. Therefore the single-bead reactor concept is embedded in the closed-loop work flow shown in Figure 23.19. Starting with the Split & Pool-method, suitable libraries of single beads can be prepared very efficiently. This preparation includes the variation of compositional parameters as well as process parameters in potential pre- and post-treatment steps, such as calcination or steaming. The resulting library is a batch of different materials, where the identity of a single bead is usually not known unless tagging is carried out during the sequential preparation steps.

In the next step, the pooled library is transferred to the single-bead reactor, where each microreaction chamber is filled with one bead. Thus the elements of the former pool are now individually *spatially addressable* in the reactor. This combination of pooled and parallel strategy allows the acquisition of performance data for each bead individually in the next processing steps. First, the catalysts are tested under continuous flow and *steady state conditions* in the single-bead reactor, where a set of different *process conditions* (reactant concentrations, residence time, temperature, etc.) is usually applied. At this stage, spatially resolved fast sequential or parallel analysis methods can be used to characterize the product composition and to identify hits.

Then the composition of a selection of or all the individual beads is determined by *X-ray fluorescence analysis* with a focused beam ( $\mu$ -XRF), which allows the identification of the *elemental composition* according to the synthesis procedure. The elemental composition of the beads can be used for tagging and also contains information about the synthesis sequence that was applied to an individual bead. Depending on the time needed for this analysis, only a subset of the library is analyzed to avoid bottlenecks.

The data generated and acquired in the previous steps is submitted to data analysis and modeling in order to generate recommendations and predictions for the preparation of the next library generation. Here, *neural networks* and *evolutionary algorithms* are used.



Beyond this work flow, single-bead reactor architecture can be used as “*integrated materials chip*.” The chip serves not only as a reactor, but also as a sample holder for the  $\mu$ -XRF characterization. Conveniently, the library can also be archived in the chip and reused later after further processing or regeneration steps or in another reaction.

## ANALYTICAL CONCEPTS FOR HIGH-THROUGHPUT PRIMARY SCREENING

### Spatially Resolved Sampling

A key component of high-throughput catalyst screening systems is a suitable product analysis technique. The number of parallel reactors in catalyst screening is, in most cases, limited by the speed of the product analysis.

Therefore a sequential *sampling device* was developed [21], shown schematically in Figure 23.20. The device consists of a *capillary probe*, which can be micropositioned in *xyz direction* within the parallel reactor configuration. The capillary probe transfers the samples to an appropriate analytical instrument [e.g., a mass spectrometer (MS), a gas chromatograph (GC), or a GC-MS]. In the present study, a conventional commercially available MS (Hiden Analytical, Warrington, UK) was used. The gas samples were continuously transferred to the MS through the capillary, allowing fast on-line analysis.

The capillary can be positioned with high accuracy under hazardous chemical conditions and high thermal demands. The parameters and the position of the capillary, which can be adjusted and monitored by a CCD camera equipped with magnifying optics, are

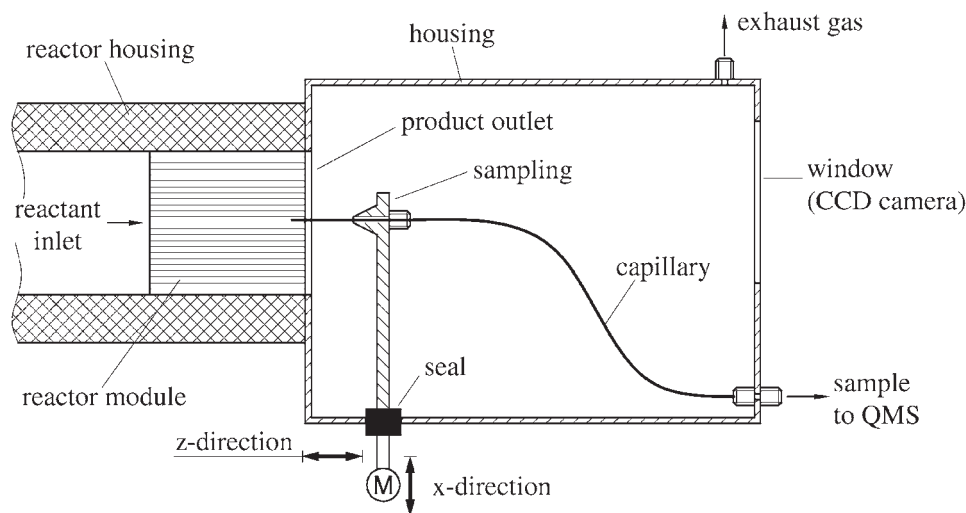


FIGURE 23.20. Sketch of the sampling device developed for spatially resolved gas analysis. The gas samples are taken sequentially by the *xyz*-positioned capillary probe and transferred to the analytical instrument (e.g., a mass spectrometer).

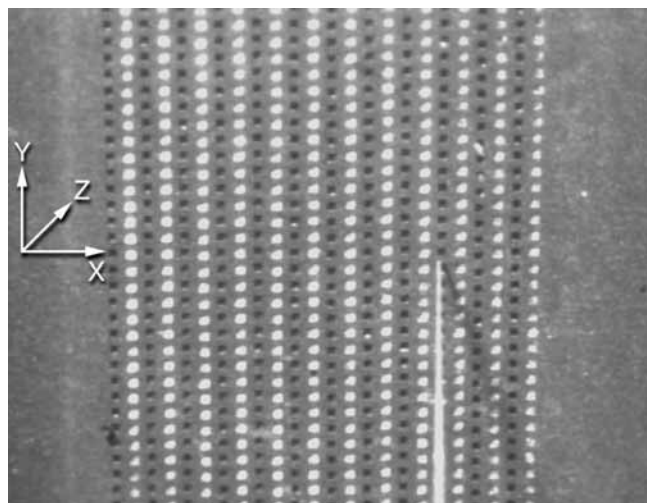
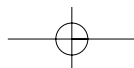


FIGURE 23.21. The microchannel array and the capillary probe of the sampling device.

freely programmable. The materials of the housing and the seal were carefully chosen to withstand temperatures up to 450°C. The speed of analysis can be determined by choosing the right MS conditions and the application of short narrow transfer capillaries. Depending on the nature of the products to be investigated, analysis times of less than 60 s can easily be achieved.

In primary screening, miniaturization is essential to increase the number of catalysts tested. The question was how far the catalytic reactors could be miniaturized while maintaining a good analysis speed and sample purity with the sampling technique described. An arrangement of microchannels was used to investigate the spatial and analytical resolution of the instrument. The outlet of the microchannel array consisted of a very large number of parallel microchannels with a cross-section of  $100\ \mu\text{m} \times 100\ \mu\text{m}$  on a pitch of only  $200\ \mu\text{m}$ . Each of these microchannels delivered a separate gas stream. The composition the substreams was analyzed using this spatially resolved analysis technique. A CCD picture of the channel outlets is shown in Figure 23.21 where lines of light and dark channel outlets can be observed resulting from light reflection due to different outlet angles. During an experiment, microchannels with light channel outlets deliver argon while those with black channel outlets deliver nitrogen. The capillary scanning the microchannels at a distance of  $50\ \mu\text{m}$  can be seen on the right-hand side of Figure 23.21.

A sampling capillary with an outer diameter of  $30\ \mu\text{m}$  and an inner diameter of  $20\ \mu\text{m}$  is used. In a typical experiment, the capillary scanned the fluid composition at different positions and distances from the channel outlets. The MS continuously analyzed the samples at a rate of about three samples per second, resulting in about 60,000 data sets per experiment. The fluid temperature was kept constant at 25°C.

A typical result obtained by scanning of the microchannel array in the  $x$  direction at a defined distance of  $50\ \mu\text{m}$  is shown in Figure 23.22. The diagram shows the molar concentration of argon in the fluid versus the capillary position. Strong variations in the argon

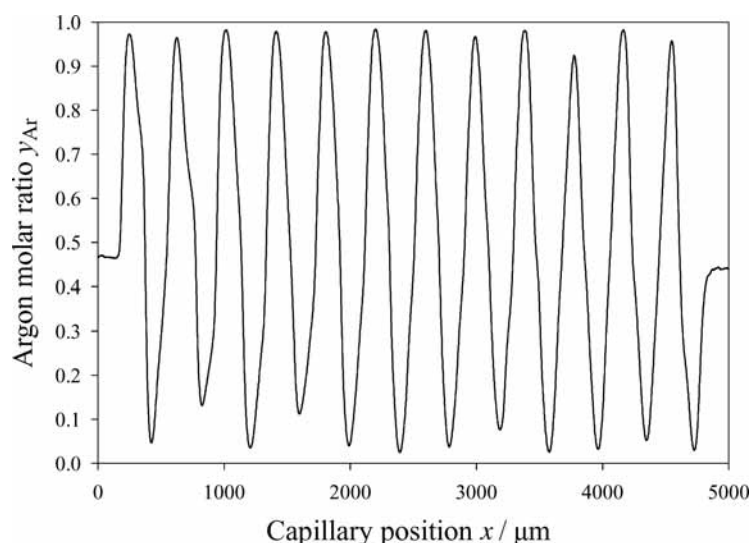


FIGURE 23.22. Screening result at  $\dot{V} = 5,000 \text{ ml min}^{-1}$  per fluid, a capillary distance of  $50 \mu\text{m}$  from the channel outlets, a capillary velocity of  $2.5 \mu\text{m s}^{-1}$ , and a temperature of  $25^\circ\text{C}$ .

concentration can be observed. The variations are very regular, representing the structure of the microchannel array at the outlet. When the capillary reaches the front of a microchannel delivering argon, the argon concentration increases to a value of almost unity. Similarly, the argon concentration decreases to almost zero when the capillary moves to a microchannel with a nitrogen substream. This illustrates that even an extremely miniaturized reactor array on a pitch of  $200 \mu\text{m}$  can be screened by means of the sampling capillary while still yielding almost pure samples.

It is obvious that parallel gas streams may mix very quickly when flowing into a common fluid chamber as an array of such microchannels acts as static micromixer. This is illustrated in Figure 23.23. When the microchannel array is scanned at a distance of  $550 \mu\text{m}$  from the outlets, the gas streams are almost completely mixed so that separate analysis of the streams is impossible. Consequently, the probe should be positioned as close as possible to the outlet of the corresponding reaction chamber. Furthermore, it may prove invaluable to take additional precautions to avoid mixing the product stream with adjacent streams at the sampling position by carefully designing the reactor outlets.

Based on our experience, a combination of the sampling device with an appropriate analysis technique can be regarded as an almost universal *sequential analysis* tool for gas phase reactions in combinatorial catalysis. The device can be used in combination with conventional commercially available analytical equipment (e.g., *MS*, *GC*, and *GC-MS*) and with almost every reactor configuration and application requiring temporally and spatially resolved sampling and the analysis of complex gaseous mixtures. In several applications, such an *xyz*-sampling device can present a significant advantage compared to channel selection *via multi-position valves*.

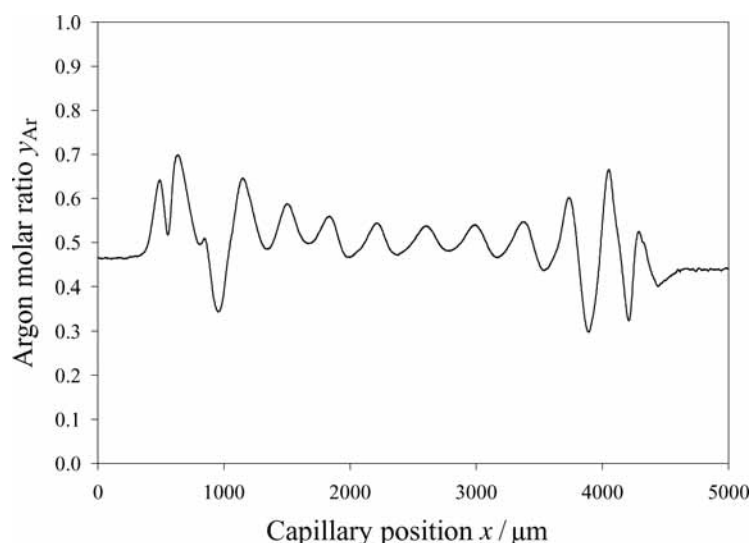
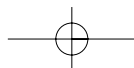


FIGURE 23.23. Screening result at  $\dot{V} = 5,000 \text{ ml min}^{-1}$  per fluid, a capillary distance of  $550 \text{ } \mu\text{m}$  from the channel outlets, a capillary velocity of  $2.5 \text{ } \mu\text{m s}^{-1}$ , and a temperature of  $25^\circ\text{C}$ .

### Parallel and Quasiparallel Product Analysis by Photoacoustics

Sequential analysis may be too slow for the reliable comparison of different catalysts in a primary screening involving several hundred catalysts operated in parallel. Therefore an effective test method has to be *real-time parallel* or *quasiparallel* to accumulate information about activity of all catalysts at the same time. We have developed a parallel detection system which is based on the *photoacoustic effect* [51]. It is based on the detection of pressure pulses, which are generated by exciting a selected type of molecule with a laser pulse. The wavelength of the laser determines which molecules are excited, because they must have an absorption band at this frequency. The molecule absorbs energy and produces a pressure pulse (if the laser is pulsed or modulated) by internal radiationless conversion of the energy into molecular translation. The intensity of the pressure pulse is correlated with the concentration of the product.

In order to demonstrate the versatility of this system, we evaluated this method in two different setups, the real parallel “*free-field setup*” and the quasiparallel “*resonance setup*.”

#### Free-Field Setup

For molecules with a high *extinction coefficient* and therefore strong light-matter interactions we developed a cell arrangement for parallel on-line detection of up to eight gas flows, which can in principle be expanded to more channels (Figure 23.24). Information on the concentration is obtained from the intensity of the pressure pulse, and information on the position of the channel is obtained by measuring the time delay

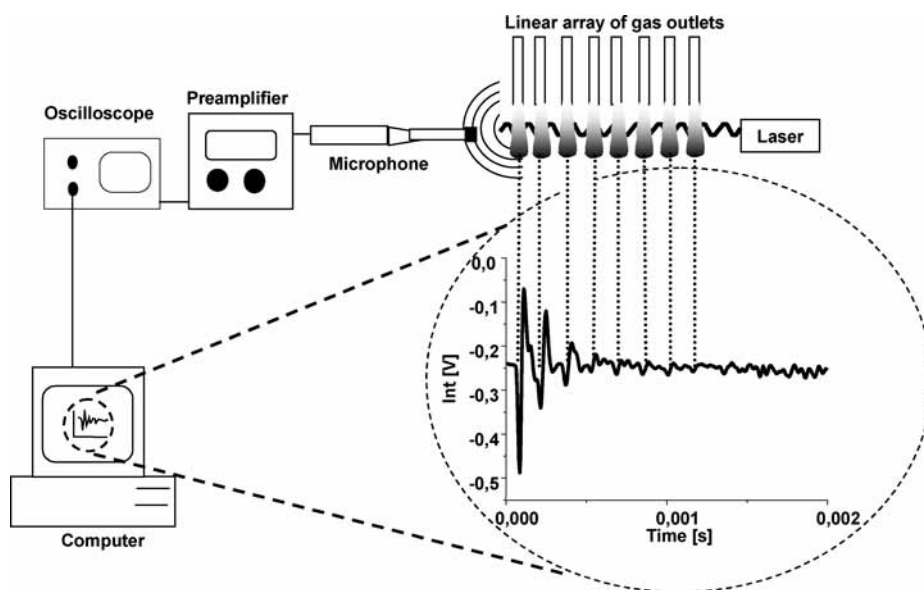


FIGURE 23.24. Free-field setup for the parallel detection of products from parallel experiments by photoaoustics.

between the laser pulse and the pressure pulse detected at the *microphone*. The spatial resolution of the setup depends on the damping of the microphone and the length of the *excitation pulse*. A spatial resolution in the centimeter range can be achieved with this setup. In our model reaction system, the *oxidative dehydrogenation* of ethane, we could easily detect ethene in an ethane–air–water background because of the strong nonoverlapping band of ethene at around  $950\text{ cm}^{-1}$ . The gas is excited by a modulated DEOS 25 W  $\text{CO}_2$  laser which was operated at 10 or 100 Hz and a pulse length of  $35\ \mu\text{s}$ . The pressure wave generated, which contains the information about the position and the concentration of ethene in all gas flows at the same time, is detected by a commercial condenser microphone. The signal from the microphone was recorded on an oscilloscope and then read out by a computer. For the free-field setup, a linear correlation of product concentration and signal intensity was proven experimentally.

To improve the signal-to-noise ratio, the oscilloscope was operated in an averaging mode, adding the response of 256 single laser pulses. An automatic peak-detection and integration routine produced a direct illustration of the conversion to ethane on-line on screen. We attached this detection cell to a 16-channel parallel reactor and were able to accumulate the complete data set of concentrations of ethene in eight gas flows within 3 s. The long measurement time is due to the averaging of 256 spectra for one measurement and the communication between the amplifier and the computer. Physically, one measurement takes only a few milliseconds.

The time difference between the signals gives a maximum spatial resolution of less than 3 cm, which could be improved by further reducing the pulse length of the laser to

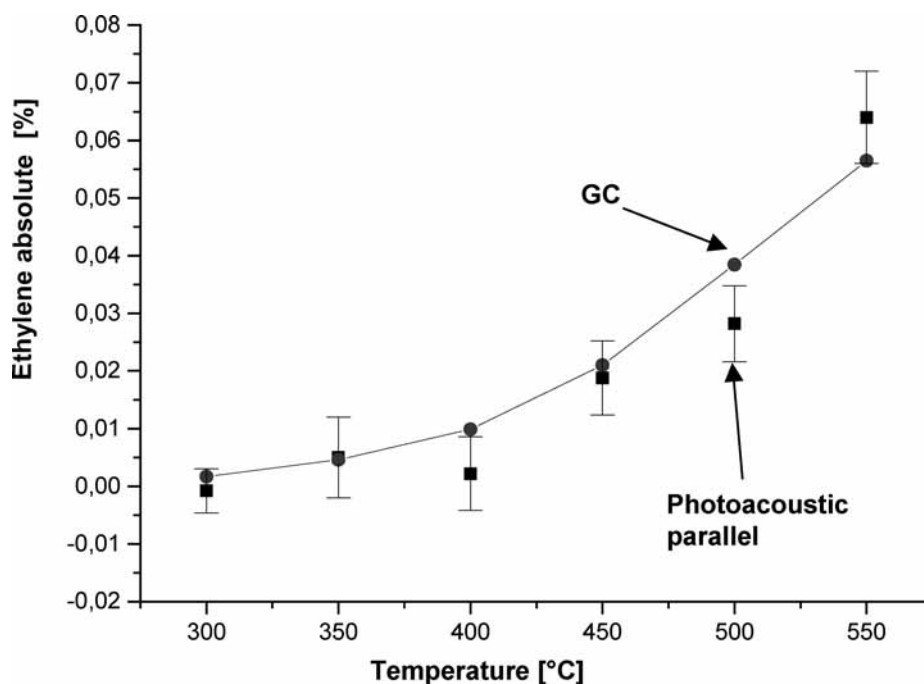
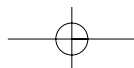
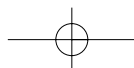


FIGURE 23.25. Analysis results from a photoacoustic parallel detection compared with a single-channel reactor with GC analysis.

reduce the propagating pressure pulse to a minimum and increasing the sensitivity of the microphone and its damping characteristics. However, this resolution was sufficient for our purpose of evaluating the applicability of the free-field measurement, since the outlets were arranged in a line with equal spacing of 5.3 cm between neighboring gas channels. For the best spatial resolution, the damping of the microphone has to be strong enough to reduce the oscillation to the offset level within the time that the pressure pulse of the next channel is detected, which is especially important for the channels close to the microphone where high pressure intensities are typically recorded. For the channels which are further away from the microphone, the damping should be low enough to detect the pulse which is reduced by  $1/r^2$ . We investigated different filters and found that a filter with low level of 20 Hz and an upper level of 30 or 100 kHz was best for the detection of all pulses.

When operating the system in an averaging mode, the lower detection limit is below 0.015% for the channels close to the microphone, and 0.3% ethane can be detected even at the remote channels where the intensity is decreased by  $1/r^2$ . Several small libraries of mixed oxide catalysts were analyzed using the photoacoustic detection method and the results were compared with those obtained in a single-channel reactor equipped with GC analytics [51]. The agreement was excellent (Figure 23.25), which proves that the method can be used for the reliable analysis of strongly absorbing molecules in a truly parallelized fashion in the free-field setup. No special requirements with respect to noise reduction in the environment are necessary.



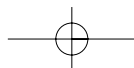
## Resonance Setup

The free-field setup cannot be used for molecules with low extinction coefficients because of the low intensity of the pressure pulses which cannot be detected by microphones with the damping characteristics necessary for the required time resolution. These very fast microphones usually have low detection limits. However, by increasing the diameter of the microphone membrane one can easily optimize the sensitivity at the expense of decreased time resolution. Therefore for CO oxidation processes with a very low extinction coefficient of CO<sub>2</sub> we had to change the detection method and give up spatial resolution and truly parallel detection.

Instead we amplified the signals from each channel by means of *resonance tubes* integrated at the end of each channel in the gas outlet [52]. These can be arranged parallel in one line and therefore are suitable for *quasiparallel* operation without complex guidance and alignment of the laser beam. With this setup, we were able to construct a system containing up to 16 tubes next to each other within 50 cm. To increase the length of the absorption path short additional horizontal tubes were attached to the resonance tube. These tubes were equipped with ZnSe windows on one side to avoid cross-contamination between the different channels which could result from diffusion out of the open tubes. Resonance conditions for the different tubes are not exactly identical because of the different conditions (i.e., beam divergence and different gas mixtures) which needed to be corrected. Each tube was equipped with a microphone, and the whole array was connected to a lock-in amplifier which was sequentially switched from channel to channel. By operating the amplifier in a phase-angle-dependent mode, we could suppress the phase of a second superimposing constant wave generated by the absorption of the tubes and detect only the signal generated by the product molecules.

With this system attached to a 16-parallel reactor, we were able to monitor 16 CO<sub>2</sub> concentrations in less than 1 min. The rate-limiting factor for these measurements is the dead-time of the switching process due to the lock-in amplifier, and not the analysis itself which is completed in less than 1 s. The reliability of this resonance detection method was checked against results from a single-channel reactor equipped with non-dispersive IR analysis and found to be in excellent agreement [51].

If there is one product which provides a characteristic *absorption band* in a frequency range which is accessible by laser sources, the *photoacoustic method* described here is a fast alternative to other methods like GC or MS. Of course, photoacoustic detection only allows information to be obtained about the *absorbing species*, whereas the whole product spectrum can be analyzed with GC or MS. For routine applications one has to choose either fast real-time detection (typically in the discovery mode) or a method delivering information about the complete product distribution which is more typical of the optimization mode. The shortcomings of the photoacoustic detection are possible overlap of absorption bands of different molecules and the fact that in the IR, which is the most convenient frequency range to use since many specific relatively narrow absorption bands are present, high-power laser sources are limited. However, the whole frequency range in the mid-IR can be covered with solid state lasers, albeit at reduced intensity and a high cost.



## SUMMARY

As a result of an interdisciplinary research effort, we have developed a novel concept for high-throughput primary screening in heterogeneous catalysis. Based on the idea of using individual shaped bodies or “beads,” as the catalytic materials of interest, a new parallel reactor type was developed. This microfabricated “single-bead reactor” can accommodate large numbers of catalytic beads in individual microreaction chambers. By using CFD calculations it was possible to achieve the design goal of a very compact arrangement of reaction chambers together with an intrinsic scalable method for equal reactant distribution. Therefore a 384-parallel single-bead reactor could be realized as a chip-based device with an overall size less than half that of a credit card. Several experiments proved the applicability of the new reactor concept in partial hydrogenation and partial oxidation reactions.

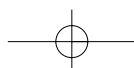
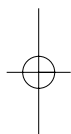
The single-bead concept allows invaluable flexibility in terms of library preparation. An outstanding feature is the possibility of applying the “Split & Pool” strategy for the synthesis of large diverse catalyst libraries in high-throughput discovery programs in heterogeneous catalysis. By applying combination of a pooled synthesis strategy and a parallel screening methodology, a very efficient automated work flow was established.

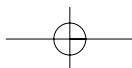
Furthermore, suitable product analysis techniques for primary screening were developed. Among the fast sequential methods, spatially resolved sampling combined with mass spectrometry proved to be a versatile tool for fast and selective analysis in very compact reactor configurations. An even higher speed of analysis can be reached by applying photoacoustic detection in a real-time parallel or quasiparallel mode.

These technologies have a number of potential applications in high-throughput experimentation in general, and primary screening in particular.

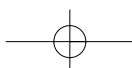
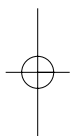
## REFERENCES

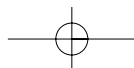
1. Lebl, M. Parallel personal comments on classical papers in combinatorial chemistry. *J. Comb. Chem.* **1999**, *1* (1), 3–24.
2. Hanak, J. J. The “multi-sample concept” in materials research: Synthesis, compositional analysis and testing of entire multicomponent systems. *J. Mater. Sci.* **1970**, *5*, 964–971.
3. Milberger, E. C. *Automatic Catalyst Screening Unit*, US Patent 4,099,923, to The Standard Oil Company, **1977**.
4. Perez-Ramirez, J., Berger, R. J., Mul, G., Kapteijn, F., Moulijn, J. A. The six-flow reactor technology—A review on fast catalyst screening and kinetic studies. *Catal. Today* **2000**, *60*, 93–109.
5. Xiang, X.-D., Sun, X., Briceño, G., Lou, Y., Wang, K.-A., Chang, H., Freedman, W. G. W., Chen, S.-W., Schultz, P. G. A combinatorial approach to materials discovery. *Science* **1995**, *268*, 1738–1740.
6. Moates, F. C., Somani, M., Annamalai, J., Richardson, J. T., Luss, D., Willson, R. C. Infrared thermographic screening of combinatorial libraries of heterogeneous catalysts. *Ind. Eng. Chem. Res.* **1996**, *35*, 4801–4803.
7. Senkan, S. M. High-throughput screening of solid-state catalyst libraries. *Nature* **1998**, *394*, 350–353.
8. Holzwarth, A., Schmidt, H.-W., Maier, W. F. Detection of catalytic activity in combinatorial libraries of heterogeneous catalysts by IR thermography. *Angew. Chem. Int. Ed.* **1998**, *37* (19), 2644–2647.
9. Cong, P., Doolen, R. D., Fan, Q., Giaquinta, D. M., Guan, S., McFarland, E. W., Poojary, D. M., Self, K., Turner, H. W., Weinberg, W. H. High-throughput synthesis and screening of combinatorial heterogeneous catalyst libraries. *Angew. Chem. Int. Ed.* **1999**, *38* (4), 483–488.





10. Jandeleit, B., Schaefer, D. J., Powers, T. S., Turner, H. W., Weinberg, W. H. Combinatorial materials science and catalysis. *Angew. Chem. Int. Ed.* **1999**, *38* (17), 2494–2532.
11. Newsam, J. M., Schüth, F. Combinatorial approaches as a component of high-throughput experimentation (HTE) in catalysis research. *Biotechnol. Bioeng. (Comb. Chem.)* **1998/1999**, *61* (4), 203–216.
12. Orschel, M., Klein, J., Schmidt, H.-W., Maier, W. F. Detection of reaction selectivity on catalyst libraries by spatially resolved mass spectrometry. *Angew. Chem. Int. Ed.* **1999**, *38* (18), 2791–2794.
13. Senkan, S., Krantz, K., Ozturk, S., Zengin, V., Onal, I. High-throughput testing of heterogeneous catalyst libraries using array microreactors and mass spectrometry. *Angew. Chem. Int. Ed.* **1999**, *38* (18), 2794–2799.
14. Hoffmann, C., Wolf, A., Schüth, F. Parallel synthesis and testing of catalysts under nearly conventional testing conditions. *Angew. Chem. Int. Ed.* **1999**, *38* (18), 2800–2803.
15. Hoffmann, C., Schmidt, H.-W., Schüth, F. A multipurpose parallelized 49-channel reactor for the screening of catalysts: Methane oxidation as the example reaction. *J. Catal.* **2001**, *198*, 348–354.
16. Senkan, S. M., Ozturk, S. Discovery and optimization of heterogeneous catalysts by using combinatorial chemistry. *Angew. Chem. Int. Ed.* **1999**, *38* (6), 791–795.
17. Liu, Y., Cong, P., Doolen, R. D., Turner, H. W., Weinberg, W. H. High-throughput synthesis and screening of V–Al–Nb and Cr–Al–Nb oxide libraries for ethane oxidative dehydrogenation to ethylene. *Catal. Today* **2000**, *61*, 87–92.
18. Reddington, E., Sapienza, A., Gurau, B., Viswanathan, R., Sarangapani, S., Smotkin, E. S., Mallouk, T. E. Combinatorial electrochemistry: A highly parallel, optical screening method for discovery of better electrocatalysts. *Science* **1998**, *280*, 1735–1737.
19. Brenner, A., de Oliveira, A. L., Schüth, F., Schunk, S. A., Stichert, W., Unger, K. *Verfahren zum Nachweis eines Produktes im Abstrom eines katalytischen Materials einer Vielzahl von katalytischen Materialien*, German Patent DE 19,830,607 to hte Aktiengesellschaft, July **1998**.
20. Busch, O., Hoffmann, C., Johann, T., Schmidt, M., Strehlau, W., Schüth, F. Application of a new color detection based method for the fast parallel screening of DeNOx catalysts. *J. Am. Chem. Soc.* **[in press]**.
21. Zech, T., Lohf, A., Golbig, K., Richter, T., Hönicke, D. Simultaneous screening of catalysts in microchannels: Methodology and experimental setup. In W. Ehrfeld (Ed.), *Microreaction Technology: Industrial Prospects, IMRET3: Proceedings of the Third International Conference on Microreaction Technology*, **2000**, Berlin: Springer-Verlag, pp. 260–266.
22. Ajmera, S., Delattre, C., Schmidt, M., Jensen, K. Microfabricated differential reactor for heterogeneous gas phase catalyst testing. *J. Catal.* **2002**, *209*, 401–412.
23. Ajmera, S. K., Delattre, C., Schmidt, M. A., Jensen, K. F. Microfabricated cross-flow chemical reactor for catalyst testing. *Sens. Actuators B* **2002**, *82*, 297–306.
24. Bergh, H. S., Engstrom, J. R., Hagemeyer, A., Lugmair, C., Self, K., Erden, L. V., Cong, P., Guan, S., Liu, Y., Markov, V., Turner, H., Weinberg, W. H. High-throughput screening of combinatorial heterogeneous catalyst libraries. Presented at IMRET4: 4th International Conference on Microreaction Technology, Topical Conference Proceedings, Atlanta, GA, AIChE National Spring Meeting, **2000**.
25. Bergh, S. H., Guan, S. *Chemical Processing Microsystems, Diffusion-Mixed Microreactors and Methods for Preparing and Using the Same*, World Patent WO 00/51720 to Symyx Technologies Inc., **1999**.
26. Zech, T. *Miniaturisierte Screening-Systeme für die kombinatorische heterogene Katalyse*, Dissertation, Technische Universität Chemnitz, VDI-Verlag Düsseldorf, Reihe 3, Nr. 732, **2002**.
27. Claus, P., Hönicke, D., Zech, T., Miniaturization of screening devices for the combinatorial development of heterogeneous catalysts. *Catal. Today* **2001**, *67* (4), 319–339.
28. Deutschmann, O., Schwiedernoch, R., Maier, L., Chatterjee, D. Natural gas conversion in monolithic catalysts: Interaction of chemical reactions and transport phenomena. In *Natural Gas Conversion VI, Studies in Surface Science and Catalysis 136*, **2001**, Amsterdam: Elsevier, pp. 215–258.
29. Deutschmann, O., Schmidt, L. D. Modeling the partial oxidation of methane in a short-contact-time reactor. *AIChE J.* **1998**, *44*, 2465–2477.
30. Zerkle, D., Allendorf, M., Wolf, M., Deutschmann, O. Understanding homogeneous and heterogeneous contributions to the partial oxidation of ethane in a short contact time reactor. *J. Catal.* **2000**, *196*, 18–39.
31. Rinnemo, M., Deutschmann, O., Behrendt, F., Kasemo, B. Experimental and numerical investigation of the catalytic ignition of mixtures of hydrogen and oxygen on platinum. *Combust. Flame* **1997**, *111*, 312–326.
32. de Smet, C., de Croon, M., Berger, R., Marin, G., Schouten, J. C. An experimental reactor to study the intrinsic kinetics of the partial oxidation of methane to synthesis gas in the presence of heat-transport limitations. *Appl. Catal. A* **1999**, *187*, 33.

AQ: pls,  
update



33. O'Connor, R., Schmidt, L., Deutschmann, O. Simulating cyclohexane millisecond oxidation: Coupled chemistry and fluid dynamics. *AIChE J.* **2002**, *48*, 1241–1256.
34. Vesper, G. Experimental and theoretical investigation of H<sub>2</sub> oxidation in a high-temperature catalytic microreactor. *Chem. Eng. Sci.* **2001**, *56*, 1265–1273.
35. Raimondeau, S., Norton, D., Vlachos, D. G., Masel, R. I. Modeling of high-temperature microburners. *Proc. Combust. Inst.* **2003**, *29*, 901–907.
36. Maruta, K., Takeda, K., Ahn, J., Borer, K., Sitzki, L., Ronney, P. D., Deutschmann, O. Extinction limits of catalytic combustion in microchannels. *Proc. Combust. Inst.* **2003**, *29*, 957–963.
37. Zech, T., Hönicke, D., Klein, J., Schunk, S. A., Demuth, D. A novel system architecture for high-throughput primary screening of heterogeneous catalysts. Presented at IMRET5: 5th International Conference on Microreaction Technology, Strasbourg, France, **2001**.
38. Idelchik, I. E. *Handbook of Hydraulic Resistance* (3rd ed.) **1994**, Boca Raton, FL: CRC Press.
39. Bird, R., Stewart, W., Lightfoot, E. *Transport Phenomena*, **1960**, New York: John Wiley.
40. Warnatz, J., Dibble, R., Maas, U. *Combustion: Physical and Chemical Fundamentals, Modeling and Simulation, Experiments, Pollutant Formation*, **1996**, New York: Springer-Verlag.
41. Coltrin, M., Kee, R., Rupley, F. *SURFACE CHEMKIN (Version 4.0): A Fortran Package for Analyzing Heterogeneous Chemical Kinetics at a Solid-Surface-Gas-Phase Interface*, Rep. SAND90-8003B, **1990**, Albuquerque, NM: Sandia National Laboratories.
42. Deutschmann, O., Kleditzsch, S., Correa, C., Tischer, S., Chatterjee, D., Warnatz, J. *DETCHEM, User Manual, Version 1.4.2*, **2002**. Available at <http://reaflow.iwr.uniheidelberg.de/~dmann/DETCHEM.html>.
43. *Fluent, Version 5*, **2000**, Lebanon, NH: Fluent Inc.
44. Furka, A., Bennett, W. D. Combinatorial libraries by portioning and mixing. *Comb. Chem. High-Throughput Screen.* **1999**, 105–122.
45. Lam, K. S., Lebl, M., Krchnak, V. The “one-bead–one-compound” combinatorial library method. *Chem. Rev.* **1997**, *97*, 411–448.
46. Krchnak, V., Dalton, C. Grabbing the golden bead. *Modern Drug Discov.* **2002**, *8*, 22–28.
47. Xiao, X.-Y., Zhao, C., Potash, H., Nova, M. P. Combinatorial chemistry with laser optical encoding. *Angew. Chem. Int. Ed.* **1997**, *36*, 780–781.
48. Guiles, J. W., Lanter, C. L., Rivero, R. A. A visual tagging process for mix and sort combinatorial chemistry. *Angew. Chem. Int. Ed.* **1998**, *37*, 926–992.
49. Baldwin, J. J., Horlbeck, E. G. *Synthesis of Combinatorial Libraries*, U.S. Patent 5,663,046 to Pharmacoepia Inc., **1994**.
50. Klein, J., Zech, T., Schunk, S. A. Split & Pool synthesis of functional inorganic materials, *Appl. Catal. A, Special Issue* **2003**, accepted for publication.
51. Johann, T., Brenner, A., Schwickardi, M., Busch, O., Marlow, F., Schunk, S., Schüth, F. Real-time photoacoustic parallel detection of products from catalyst libraries. *Angew. Chem. Int. Ed.* **2002**, *41* (16), 2966–2968.
52. Johann, T., Brenner, A., Schwickardi, M., Busch, O., Marlow, F., Schunk, S., Schüth, F. Listening to catalysis—A real time parallel method for high throughput product analysis. *Catal. Today* **2003**, *8* (3), 449–455.

